4 Results

4.1 Assignment of functional domains in p101

The first part of this thesis dealt with the elucidation of the domain structure of the PI3Kγ regulatory subunit p101. It commenced as the preceding diploma thesis (Voigt, 2003). To describe the mapping process in full, the first two figures present data that were already part of the diploma thesis. Aiming at the assignment of functional features of p101 to distinct regions of its primary structure, deletion mutants of p101 were generated and characterized regarding their ability to bind to p110γ and G$\beta\gamma$, the two known interaction partners of p101.

4.1.1 Establishing a sketchy functional map

First, a limited set of constructs was generated in order to establish an approximate map of p101 (Fig. 4.2*C*). Their subcellular localization was analyzed and compared to that of wild-type p101. Full-length p101 – if expressed without the catalytic p110γ subunit – is located mostly within the cell nucleus (Fig. 4.1, *upper panels*). A similar distribution was obtained for constructs lacking either the N or C terminus of p101. The nuclear localization was markedly reduced upon deletion of the center part of p101, whereas a construct comprising only aa 249–613 partitioned exclusively to the nucleus. Hence, it is likely that the center part of p101 mediates its nuclear accumulation. Indeed, analysis of the p101 primary structure using PSORTII (Nakai & Horton, 1999) revealed the existence of three nuclear localization sequences (NLS) in porcine p101. They are located at positions 400–403, 499–502, and 558–565, *i.e.* in the middle part of p101.

The catalytic p110γ subunit of PI3Kγ locates to the cytosol of HEK293 cells (Brock *et al.*, 2003; Voigt, 2003). Upon coexpression with p110γ, CFP-p101 was relocated to the cytosol and mostly excluded from the cell nucleus (Fig. 4.1, *middle panels* and Brock *et al.*, 2003), indicative of an interaction between both subunits. A similar redistribution was observed for the C-terminally truncated p101 deletion mutant CFP-p101$_{1-613}$, but not for the N-terminally truncated p101 deletion mutant p101$_{249-877}$-CFP. The shorter deletion mutants retained their cytosolic or nuclear localization. These data point to a crucial function of the p101 N terminus in the interaction with p110γ, whereas the C terminus and center parts of p101 appear to be themselves insufficient for an interaction with p110γ.

To verify these results and to be able to assess the interaction of p110γ with the p101 deletion mutants that chiefly show cytosolic localization, a FRET-based assay was used. In agreement

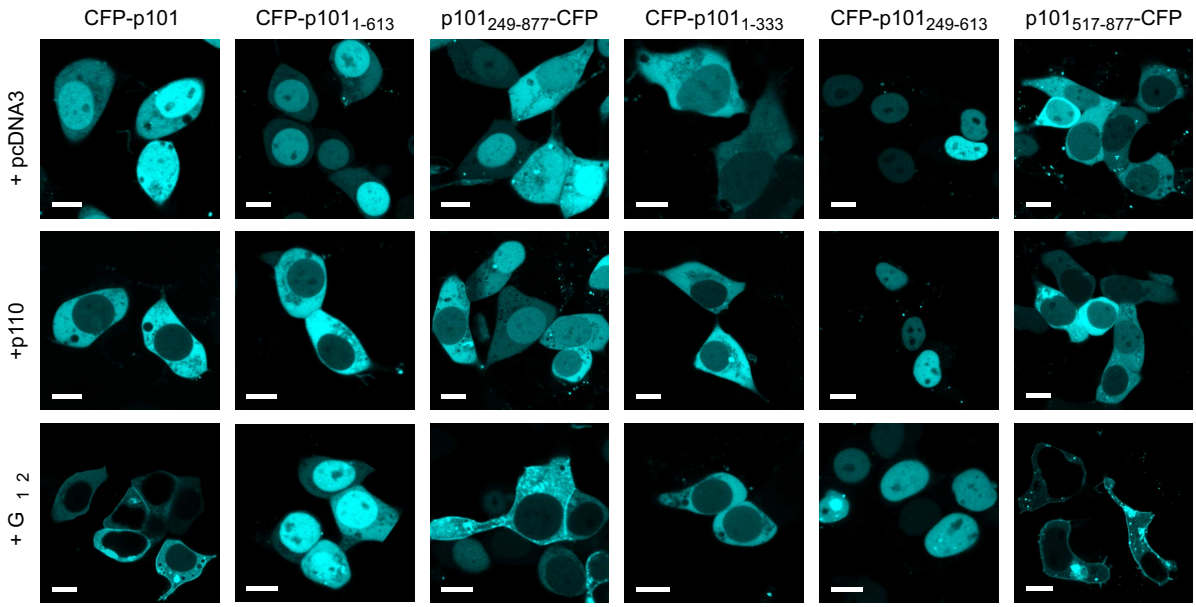

Figure 4.1: Differential subcellular localization of p101 deletion mutants upon coexpression with p110γ or G$\beta\gamma$. HEK293 cells were transfected with plasmids encoding the indicated p101 deletion mutants and either pcDNA3 (empty vector), p110γ, or Gβ_1 and Gγ_2. Cells were analyzed by confocal microscopy. Representative images are shown (bars: 10 μm). Most images in this figure were taken from the preceding diploma thesis (Voigt, 2003).

with previous studies (Brock *et al.*, 2003), a FRET efficiency of ~9% was measured between YFP-p110γ and CFP-p101 in living HEK293 cells. Fig. 4.2*A,B* shows a representative acceptor photobleach experiment. A similar FRET efficiency was obtained if YFP-p110γ was coexpressed with either CFP-p101$_{1-613}$ or CFP-p101$_{1-333}$ (Fig. 4.2*C*, *black bars*), suggesting that C-terminal parts of p101 are not required for interaction with p110γ. Moreover, fragments comprising only the middle or C-terminal parts of p101 yielded FRET efficiencies with p110γ-YFP that were comparable to those obtained upon coexpression of free CFP and p110γ-YFP (Fig. 4.2*C*, *gray bars*). Taken together, these data imply that the N terminus of p101 is both necessary and sufficient to bind p110γ, while the center and C-terminal parts are neither sufficient nor mandatory for this interaction.

The interaction of p101 deletion mutants with G$\beta\gamma$ was assessed by a recruitment assay similar to that used for analysis of the interaction with p110γ. Coexpression of CFP-p101 and G$\beta\gamma$ led to a redistribution of CFP-p101 to the plasma membrane and cytosol of HEK293 cells, whereas little fluorescence remained within the cell nucleus (Fig. 4.1, *lower panels*), indicating an interaction of p101 with the mostly membrane-localized G$\beta\gamma$ complexes. A similar impact on subcellular localization was only observed for p101$_{249-877}$-CFP and p101$_{517-877}$-CFP, *i.e.* mutants retaining the C terminus of p101. These observations suggest a central role for the C terminus of p101 in the interaction with G$\beta\gamma$, while the N terminus is not required for that interaction.

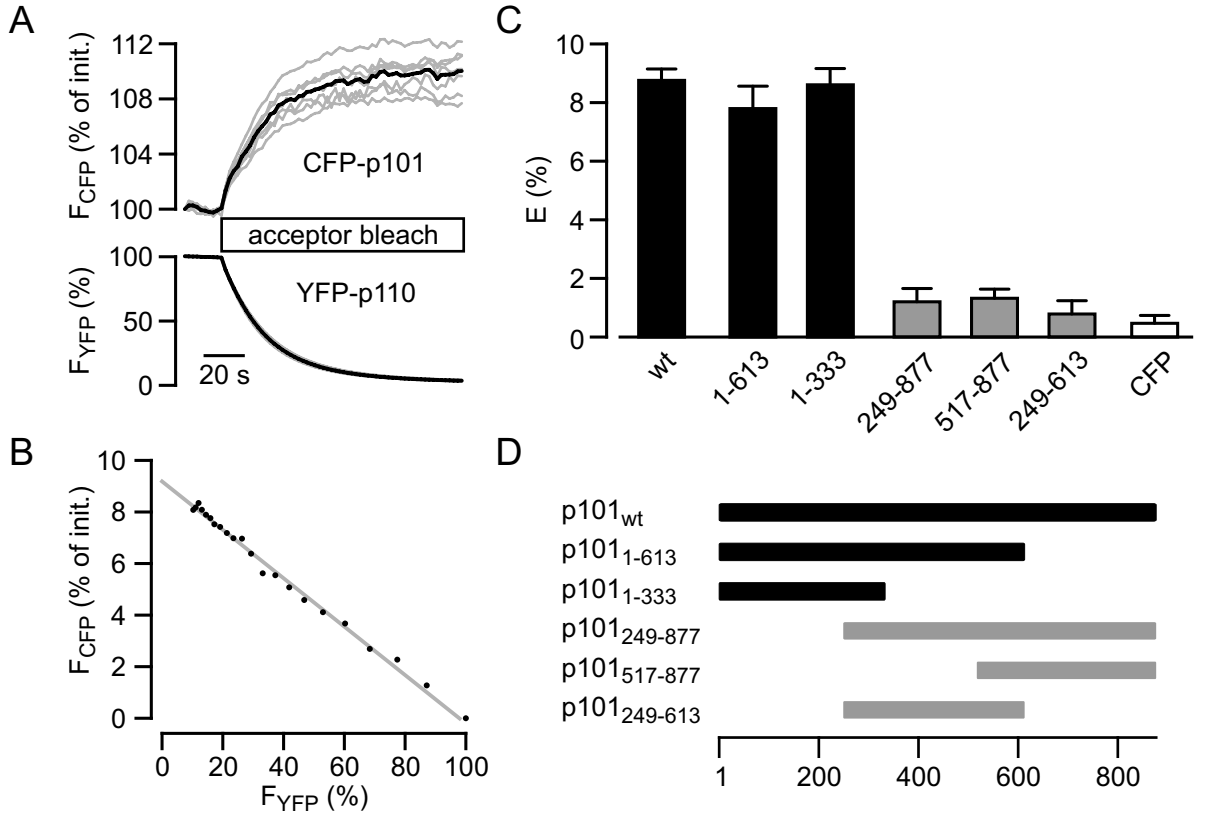

Figure 4.2: FRET between fluorescent fusion proteins of p110γ and p101 deletion mutants. *A*, single cell (gray lines) and mean (black lines) fluorescence traces of CFP and YFP acquired during a representative acceptor photobleaching protocol. Traces were normalized to the initial (init.) fluorescence intensities. The measurement shown was performed on living HEK293 cells transfected with plasmids encoding CFP-p101 and YFP-p110γ, resulting in expression at a YFP:CFP ratio of $\sim$2:1. *B*, regression analysis of the data depicted in *A*. To obtain the FRET efficiency E from the formula given in section 3.6.3, the increase in CFP fluorescence was extrapolated to complete YFP photobleach. *C*, assessment of the interaction between p101 deletion mutants and p110γ by FRET. HEK293 cells were transfected with the indicated p101 deletion mutants and YFP-p110γ. p110γ-YFP was used for C-terminally CFP-tagged p101 deletion mutants $p101_{249-877}$ and $p101_{517-877}$. For full-length p101 (wt), the CFP tag was at the N terminus. For the p101 deletion mutants, CFP was fused to the native N or C terminus of p101, if present. Data shown for $p101_{249-613}$ were obtained with an N-terminal CFP fusion. Given are means and S.E. of four independent measurements with at least six cells each. *D*, Schematic drawing of wild-type and truncated p101 constructs. The shading corresponds to that used in *C*. Part of the data shown in this figure already appeared in the preceding diploma thesis (Voigt, 2003).

Under *in vivo* conditions in an heterologous cell model, both N and C termini of p101 proved to be necessary for mediating the activation of p110γ by G$\beta\gamma$. In HEK293 cells expressing the formyl-methionyl-leucyl-phenylalanine (fMLP) receptor, p110γ, full-length p101, and the YFP-fused PIP_3-binding PH domain of Grp1 (YFP-Grp1-PH), which acts as a translocating biosensor for class I PI3K activity (Gray *et al.*, 1999), stimulation with fMLP led to a marked translocation of YFP-Grp1-PH to the plasma membrane (Fig. 4.3, *upper panels*). As indicated by the lack of

a discernible translocation of YFP-Grp1-PH, activation of p110γ was completely abrogated if p101$_{249-877}$ was expressed instead of full-length p101 (Fig. 4.3, *middle panels*). From the data described above it may be reasoned that this absence of PI3Kγ activity was due to the lack of interaction between p110γ and the N-terminally truncated mutant of p101. p101 may be recruited to the plasma membrane by G$\beta\gamma$, but cannot co-translocate p110γ. Likewise, absence of the G$\beta\gamma$-interacting C terminus of p101 abolished translocation of YFP-Grp1-PH (Fig. 4.3, *lower panels*). In this case, p101$_{1-613}$ was presumably still bound to p110γ, but unable to interact with G$\beta\gamma$ complexes.

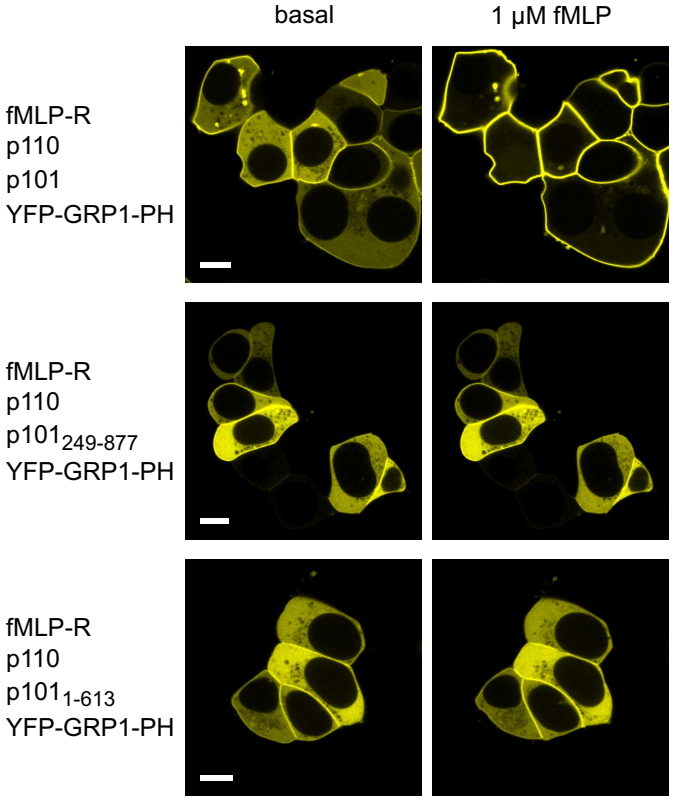

Figure 4.3: Impact of N- and C-terminal deletions within p101 on GPCR-mediated PI3Kγ activation *in vivo*. HEK293 cells were transfected with plasmids encoding proteins that reconstitute a PI3Kγ signaling pathway. The YFP-fused PH domain of Grp1 was used as a read-out for PI3Kγ activity. It is a translocating biosensor that binds to the PI3K lipid product PIP_3. The subcellular localization of YFP-Grp1-PH was monitored before and 2 min after stimulation of the cotransfected fMLP receptor (fMLP-R) by 1 μM fMLP for different settings containing either full-length or N- or C-terminally truncated versions of p101. Bars: 10 μm.

4.1.2 Fine-mapping of the p110γ binding domain

The analysis of the initially generated p101 deletion mutants indicated that the N terminus of p101 is sufficient for interaction with p110γ. Therefore, further deletion mutants were constructed to define the limits of the p110γ interaction domain within the N terminus, using a finer spacing of 25 aa (see Fig. 4.4*B* for a schematic representation).

Before commencing the mapping experiments, it was first aimed to verify that the attribution of the p110γ-interacting properties to the N terminus of p101 was not due to generation of an artificial binding site through the truncation. To this end, FRET competition assays were performed. p101-CFP was displaced from its interaction with p110γ-YFP by coexpressed wild-type untagged p101 in a concentration-dependent manner, resulting in a reduction of FRET

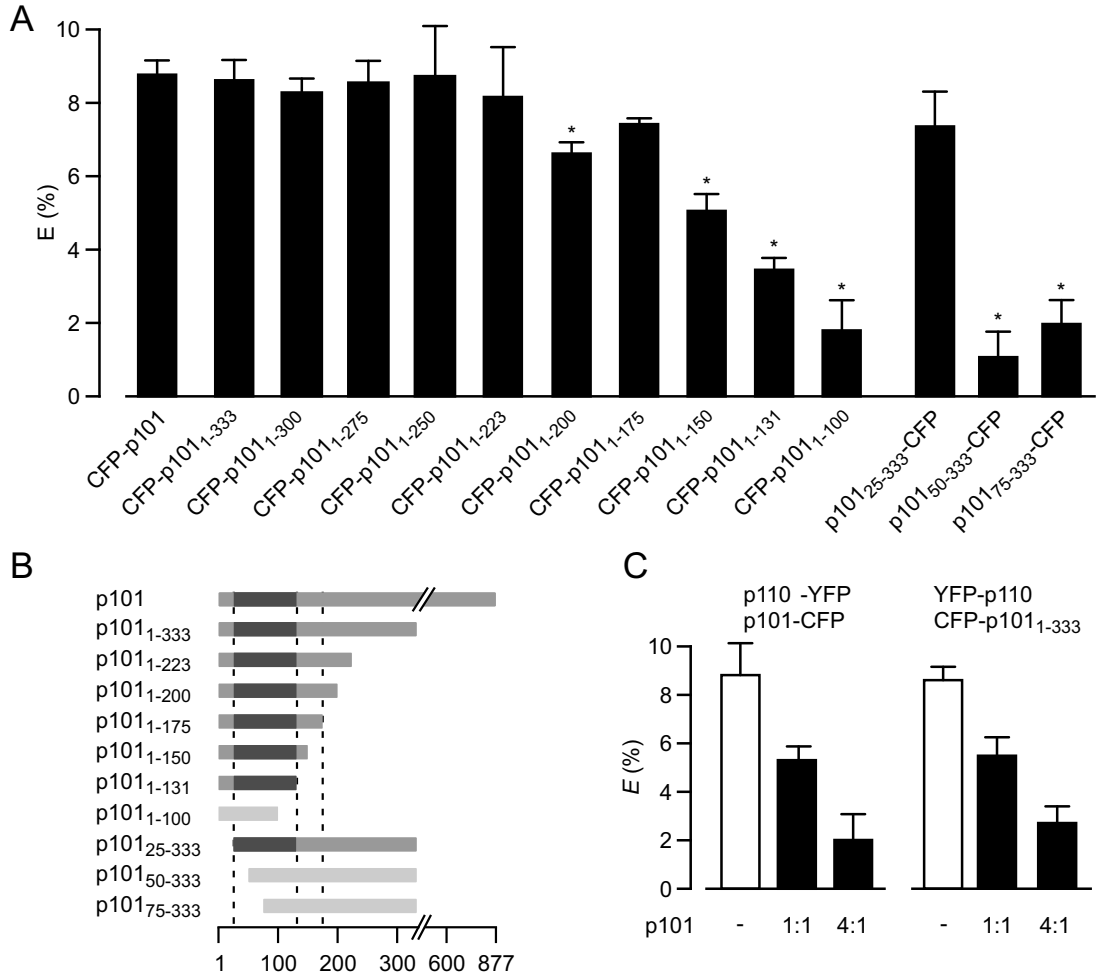

Figure 4.4: Mapping of the p110γ interaction site on p101 by FRET. *A*, FRET efficiencies between YFP-p110γ and various CFP-tagged p101 deletion mutants. HEK293 cells were transfected with plasmids encoding YFP- p110γ and the indicated p101 deletion mutant. Given are means and S.E. of four independent acceptor bleach measurements with at least six cells each. Raw data were processed as described (see section 3.6.3 and Fig. 4.2). Asterisks indicate FRET efficiencies significantly different from that for the donor–acceptor pair CFP-p101–YFP-p110γ ($p < 0.05$; unpaired Wilcoxon test). *B*, schematic overview of the N-terminal deletion mutants characterized in *A*. Shading of the boxes corresponds to the ability of the constructs to bind to p110γ, with interacting constructs in light gray and the core minimal interaction region in dark gray. *C*, competition of FRET between full-length p101-CFP and p110γ-YFP and between CFP-p101$_{1-333}$ and YFP-p110γ. HEK293 cells were cotransfected with a constant amount of the indicated plasmids encoding fluorescent proteins and increasing amounts of plasmid encoding untagged p101. The ratio between untagged p101 and CFP-tagged protein is indicated below the bars. As in *A*, means and S.E. of four independent measurements are shown.

efficiency (Fig. 4.4*C, left panel*). Likewise, the FRET efficiency obtained for CFP-p101$_{1-333}$ and YFP-p110γ was reduced to a similar extent by coexpression of untagged p101 (Fig. 4.4*C, right panel*), suggesting that both p101 and p101$_{1-333}$ share a common binding site on p110γ.

To assess the binding of the N-terminal panel of p101 deletion mutants to p110γ, first a

FRET-based mapping approach was used that allows to explore the binding interface in living cells. Based on the assumption that the environment of the CFP moiety is not significantly altered by further truncating the deletion mutant at the opposite terminus, a reduction in FRET efficiency should directly correlate with a reduction in affinity between the binding partners. Upon shortening CFP-p101$_{1-333}$ from its C terminus, the FRET efficiency remained essentially unaltered up to aa 175 (Fig. 4.4*A*). An exception was CFP-p101$_{1-200}$, which showed a small but statistically significant reduction in FRET efficiency. In shortening the constructs even further from their C terminus, significant and obvious differences were obtained for CFP-p101$_{1-150}$ and CFP-p101$_{1-131}$. An efficiency close to that determined for free CFP and p110γ-YFP (see Fig. 4.2*C*) was reached for CFP-p101$_{1-100}$, indicating a loss of binding. Upon deleting N-terminal residues from p101$_{1-333}$-CFP, only deletion of the first 25 aa was tolerated, and further deletions immediately led to complete loss of FRET efficiency with YFP-p110γ.

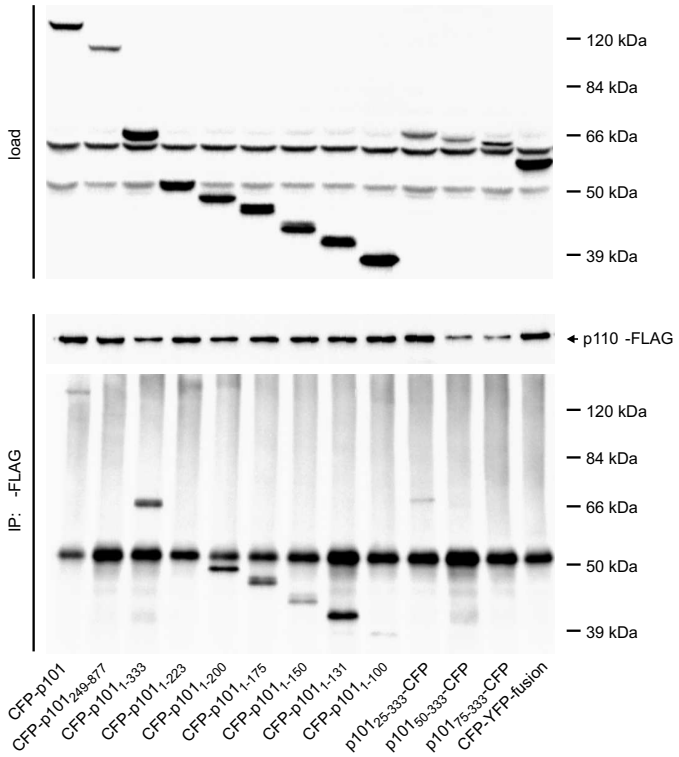

Figure 4.5: Coimmunoprecipitation of p110γ and p101 deletion mutants. HEK293 cells were transfected with plasmids coding for p110γ-FLAG and the indicated p101 deletion mutants. p110γ-FLAG was immunoprecipitated from cleared lysates with an anti-FLAG antibody. Copurified p101 deletion mutants were detected with an anti-GFP antibody (IP) and compared to the amount that was present in the cell lysates (load). Note that CFP-p101$_{1-223}$ is not visible in the respective immunoprecipitate due to an unspecific band present in all lanes.

To support the results that arose from the FRET-based approach and to test for a physical association, a conventional co-IP analysis was performed. The fragments were coexpressed with p110γ-FLAG and assayed for copurification upon IP of p110γ-FLAG. In agreement with the FRET measurements, all truncated constructs with C-terminal deletions up to aa 131 or with N-terminal deletions up to aa 25 were detectable in the immunoprecipitates (Fig. 4.5). Only a very faint signal was obtained in the precipitate for CFP-p101$_{1-100}$, indicating a loss of interaction. No signal at all was visible in the immunoprecipitate for p101$_{249-877}$-CFP, the N-terminal deletion mutants beyond aa 25, and a CFP-YFP fusion protein used as a negative

control. Hence, aa 25–131 comprise the minimal binding site of p101 for p110γ, although the sequence up to aa 175 is necessary to reach a FRET efficiency with YFP-p110γ that is comparable to that of full-length p101.

4.1.3 Fine-mapping of the G$\beta\gamma$ binding domain

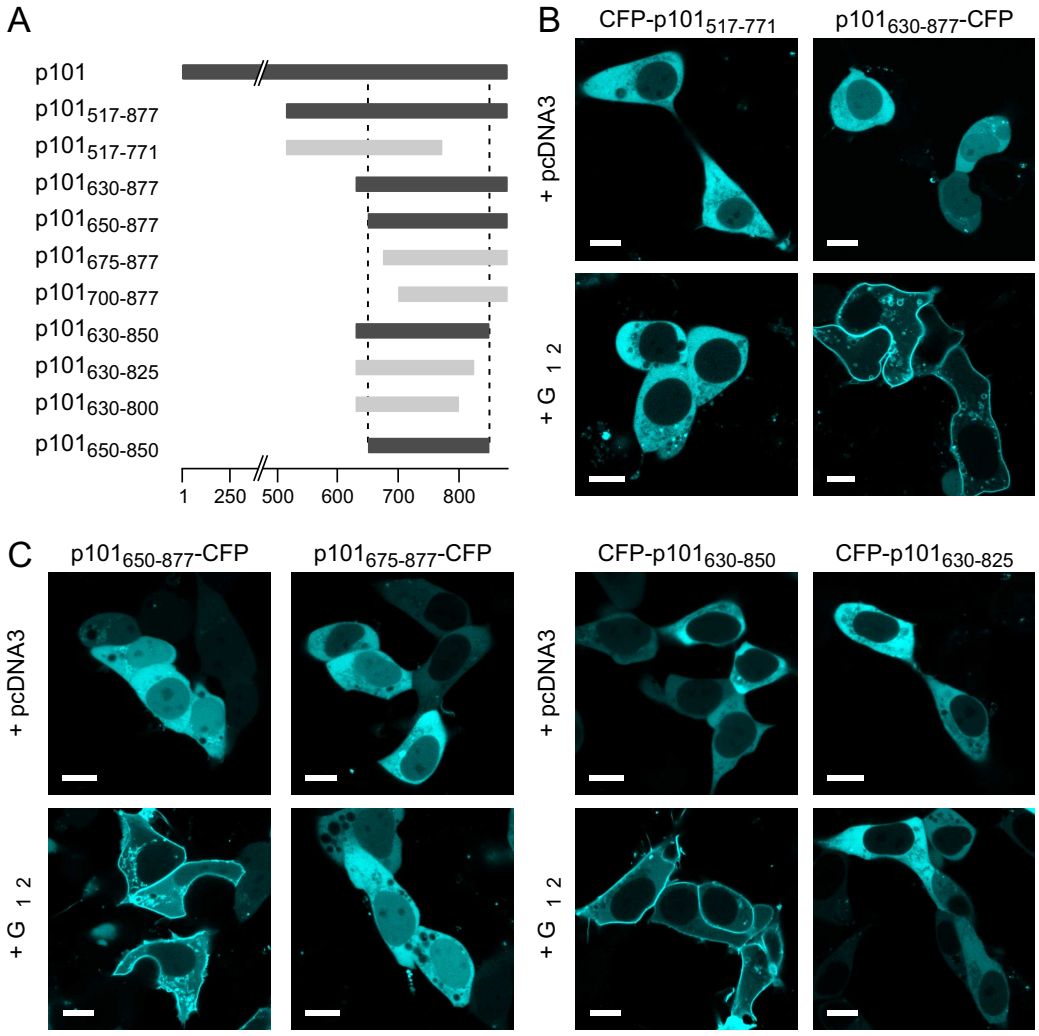

Figure 4.6: Assignment of the G$\beta\gamma$ binding site on p101. *A*, schematic overview showing the p101 deletion mutants within the C terminus of p101. Dark shading indicates constructs that are able to bind to G$\beta\gamma$. *B,C*, HEK293 cells were transfected with the indicated constructs and either empty vector (pcDNA3) or plasmids coding for Gβ_1 and Gγ_2. 1–2 days after transfection, living cells were analyzed by confocal microscopy. Representative images are shown (bars: 10 μm).

For a more accurate analysis of the G$\beta\gamma$ binding domain, the same recruitment assay as used for the initial mapping was employed (see section 4.1.1). Because the construct p101$_{517-877}$-CFP still showed binding to G$\beta\gamma$ (see Fig. 4.1), further truncated mutants within these borders were generated and analyzed (see Fig. 4.6*A* for a schematic representation).

Coexpression of G$\beta\gamma$ led to a prominent plasma membrane localization of p101$_{630-877}$-CFP but not of CFP-p101$_{517-771}$, indicating that regions within the C-terminal third of p101$_{517-877}$ are necessary for interaction with G$\beta\gamma$ (Fig. 4.6*B*). An additional 20 aa-deletion at the N terminus of p101$_{630-877}$ does not influence plasma membrane localization, whereas deletion of 45 aa led to loss of interaction with G$\beta\gamma$ (Fig. 4.6*C*, *left panels*). From the C terminus, ~25 aa may be deleted without interfering with G$\beta\gamma$ binding, but interaction with G$\beta\gamma$ was lost if ~50 aa were removed (Fig. 4.6*C*, *right panels*). Hence, these data show that sequences within aa 650–850 of p101 are both necessary and sufficient to mediate interaction with G$\beta\gamma$. Indeed, a construct comprising only aa 650–850 of p101 was still recruited from the cytosol to the plasma membrane upon coexpression of G$\beta\gamma$ (Fig. 4.7*A*). Compared to the full-length p101-YFP, the membrane localization of CFP-p101$_{650-850}$ was substantially increased. This observation may suggest a higher affinity of the isolated C-terminal G$\beta\gamma$-binding fragment for G$\beta\gamma$ compared to the full-length p101. In support of this hypothesis, CFP-p101$_{650-850}$ was able to displace p101-YFP from binding to G$\beta\gamma$ in a presumably competitive manner (Fig. 4.7*B*).

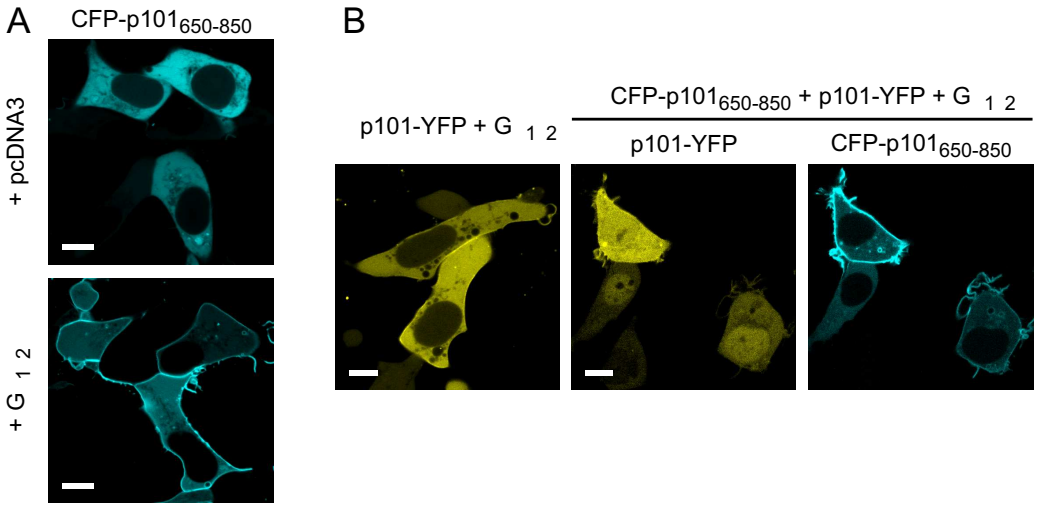

Figure 4.7: Full-length p101 and p101$_{650-850}$ compete for binding to G$\beta\gamma$. *A*, CFP-p101$_{650-850}$ interacts with G$\beta\gamma$. HEK293 cells transfected with plasmids encoding the p101 deletion mutant and either G$\beta\gamma$ or empty vector were analyzed by confocal microscopy (bars: 10 μm.) *B*, competition of binding to G$\beta\gamma$. p101-YFP was coexpressed with G$\beta\gamma$ either without (left) or together with CFP-p101$_{650-850}$ (middle and right). Note the altered subcellular localization of p101-YFP in the presence of CFP-p101$_{650-850}$ (bars: 10 μm).

4.1.4 Interference with PI3Kγ signaling

Given the independent function of the C-terminal G$\beta\gamma$ binding domain of p101, it was assumed that it may act as an isotype-specific, dominant-negative modulator of PI3Kγ signaling. Indeed, activation of PI3Kγ was profoundly inhibited in HEK293 cells in which a PI3Kγ signaling pathway has been reconstituted. As seen in Fig. 4.3, stimulation with 1 µM fMLP led

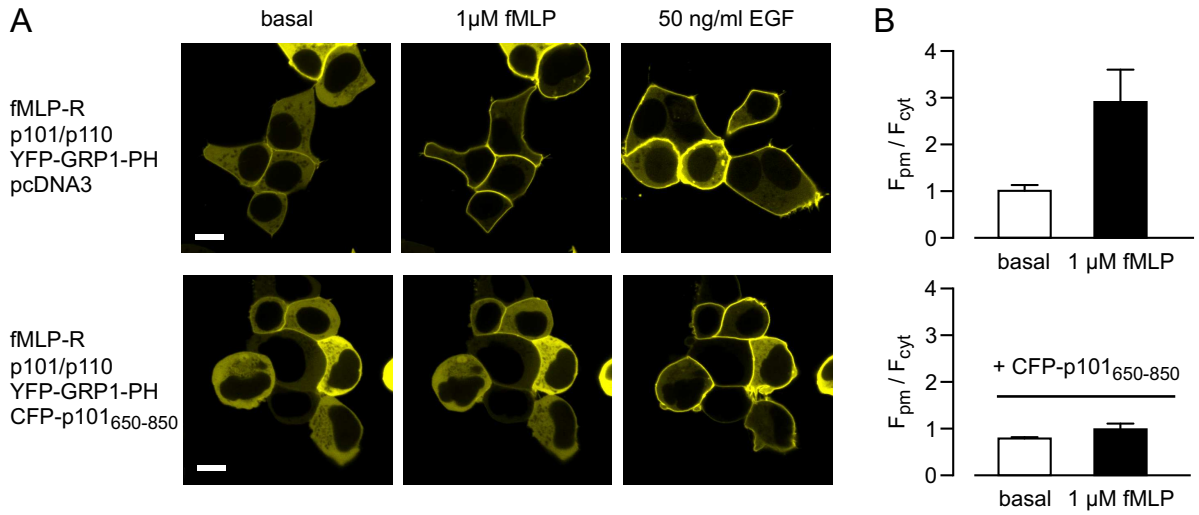

Figure 4.8: Abrogation of PI3Kγ activation through the G$\beta\gamma$ binding domain of p101. *A*, assessment of the impact of p101$_{650-850}$ coexpression on PI3Kγ activity by monitoring translocation of YFP-Grp1-PH. HEK293 cells were transfected with plasmids encoding the indicated proteins to reconstitute a PI3Kγ signaling pathway. Confocal images show the localization of YFP-Grp1-PH before and 2 min after the addition of either 1 μM fMLP or 50 ng/ml EGF (bars: 10 μm). In the upper panel, a different cell group not pre-stimulated with fMLP is shown for EGF stimulation. For the sequential stimulation shown in the lower panel, EGF was added 2 min after fMLP. *B*, statistical analysis of YFP-Grp1-PH membrane translocation. Multiple experiments conducted as shown in *A* were evaluated by defining lines over cytosol and adjacent plasma membranes of cells. From the intensity profiles along theses lines, the mean cytosol fluorescence was calculated within a homogeneous region of cytosol, and the mean plasma membrane fluorescence was defined as the mean of the maximum fluorescence intensity at both edges of the cytosol. The degree of membrane association was then expressed as the ratio of both values. Data shown are means and S.E. derived from five independent experiments with 3–6 cells each.

to a pronounced translocation of the PIP_3-binding YFP-Grp1-PH construct in HEK293 cells expressing the fMLP receptor, p110γ, and p101 (Fig. 4.8*A, upper panels*). Activation of endogenous class IA PI3Ks by stimulation with EGF led to a comparable translocation. Overexpression of CFP-p101$_{650-850}$, however, almost completely abrogated the translocation of YFP-Grp1-PH upon stimulation with fMLP, whereas the EGF-induced translocation was unaffected in the same cells (Fig. 4.8*A, lower panels*). Inhibition of PI3Kγ activity by CFP-p101$_{650-850}$ was reproducible and highly efficient in several experiments (Fig. 4.8*B*). Since class IA PI3Ks do not rely on G$\beta\gamma$ for their activation, EGF-stimulated PI3K activity is retained under the same conditions, resulting in an isotype-specific inhibition of PI3Kγ.

Considering the effect on G$\beta\gamma$-mediated activation of PI3Kγ, the impact on PLCβ enzymes was analyzed as an example for other effectors of G$\beta\gamma$. Phospholipases Cβ (PLCβ) are part of a signaling cascade that links stimulation of GPCRs to the release of Ca^{2+} from the endoplasmatic reticulum by catalyzing the cleavage of $PI(4,5)P_2$ to diacylglycerol and inositol-1,4,5-trisphosphate, which is bound by its receptor channel on the endoplasmatic reticulum. Of

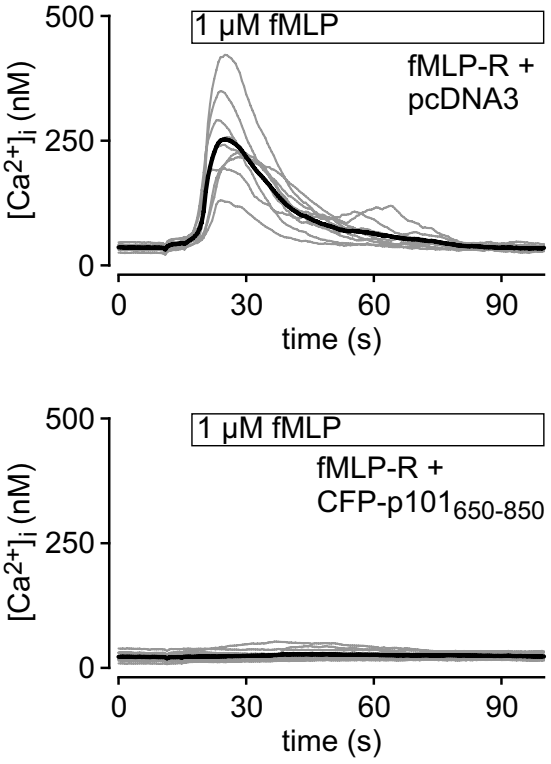

Figure 4.9: The G$\beta\gamma$ binding domain of p101 acts as a G$\beta\gamma$-scavenging protein. Changes in intracellular calcium ($[Ca^{2+}]_i$) were monitored in HEK293 cells expressing the fMLP receptor either alone or in combination with CFP-p101$_{650-850}$. Cells were loaded with the Ca^{2+}-sensitive dye fura-2 and stimulated with 1 μM fMLP. The traces shown (black for mean, gray for single cell traces) are from a representative experiment of three.

the GPCR-regulated PLC, mainly PLCβ_2 can be effectively activated by G$\beta\gamma$ complexes (Rhee, 2001). Stimulation of a G_i-coupled receptor such as the fMLP receptor leads to an increase in $[Ca^{2+}]_i$ (Fig. 4.9, *upper panel*), which is mediated by G$\beta\gamma$-sensitive PLCβ isoenzymes such as PLCβ_2. Coexpression of CFP-p101$_{650-850}$ led to an almost complete abolition of the rise in $[Ca^{2+}]_i$ (Fig. 4.9, *lower panel*), indicating a competition for released G$\beta\gamma$ subunits between CFP-p101$_{650-850}$ and endogenous PLCβ enzymes. Hence, the G$\beta\gamma$ binding domain of p101 is a potent G$\beta\gamma$-scavenging protein that binds to G$\beta\gamma$ and interferes with G$\beta\gamma$ signaling in the activation of both PI3Kγ and other effectors.

4.1.5 Conservation of the functional domains in orthologues of p101

In summary, the N terminus of p101 (aa 25–175) mediates binding to p110γ and thus constitutes the heterodimerization domain of p101, while the C-terminal region comprising aa 650–850 is responsible for binding to G$\beta\gamma$, which is therefore termed G$\beta\gamma$ binding domain (Fig. 4.10). Assuming that the signal transduction pathway is not significantly altered between species, the evolutionary pressure towards conservation of functionally relevant areas should be higher than in regions that are not critical for the protein function. Genome sequencing projects allow for an analysis of protein sequences of p101 from a large array of species. An alignment is shown in Fig. 4.11. The obviously higher degree of conservation within the N- and C-terminal functional regions of p101 as compared to the intervening sequence stretch supports the conclusions drawn from the mapping experiments. Depending on the phylogenetic distances of

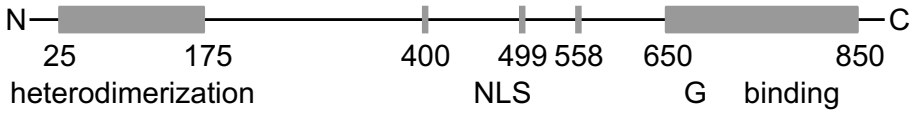

Figure 4.10: Domain structure of p101. Schematic drawing of the primary structure of p101. Boxes indicate the position of interaction domains and NLS in porcine p101. Note that only the NLS at position 499 may be functionally relevant as inferred from comparison with various orthologues of p101.

the species involved, the pairwise similarities of the overall sequences vary between 40–99%. Within the N-terminal heterodimerization domain, these similarities are higher, being in the range of 52–100% . Similarly, the pairwise similarities give higher values for the C-terminal G$\beta\gamma$ binding domain (55–100%). On the other hand, the intervening sequences are less well conserved (pairwise similarities of 29–92%).

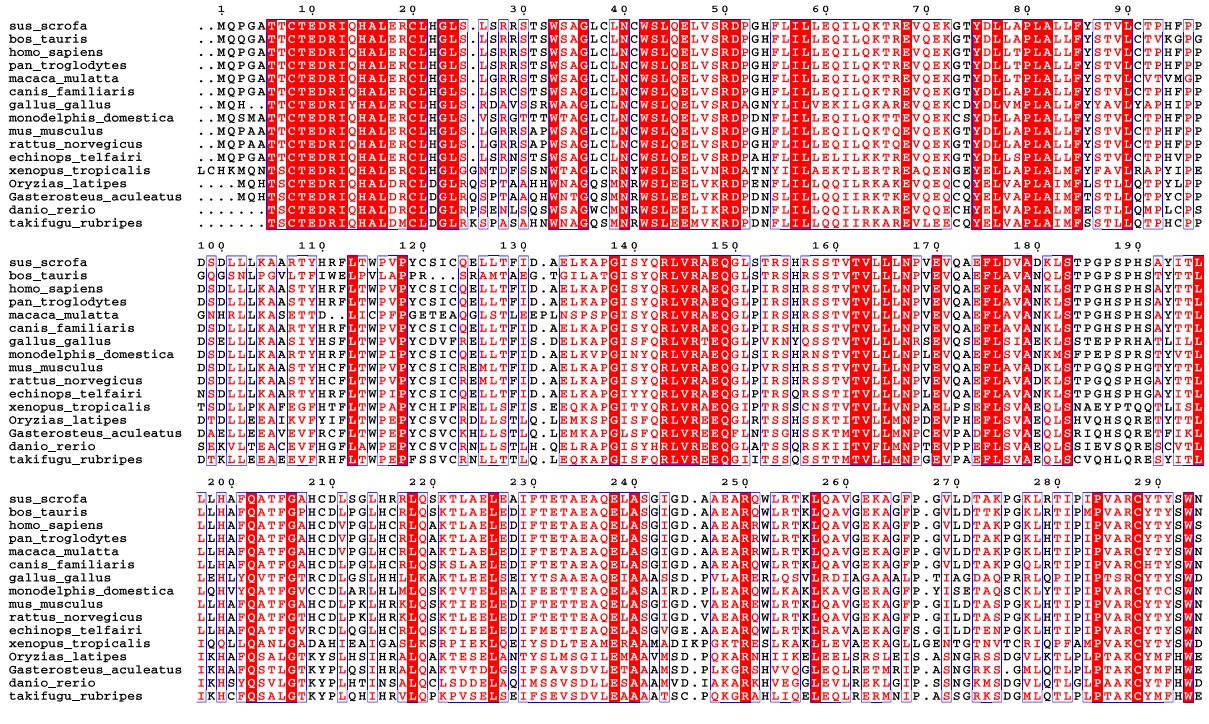

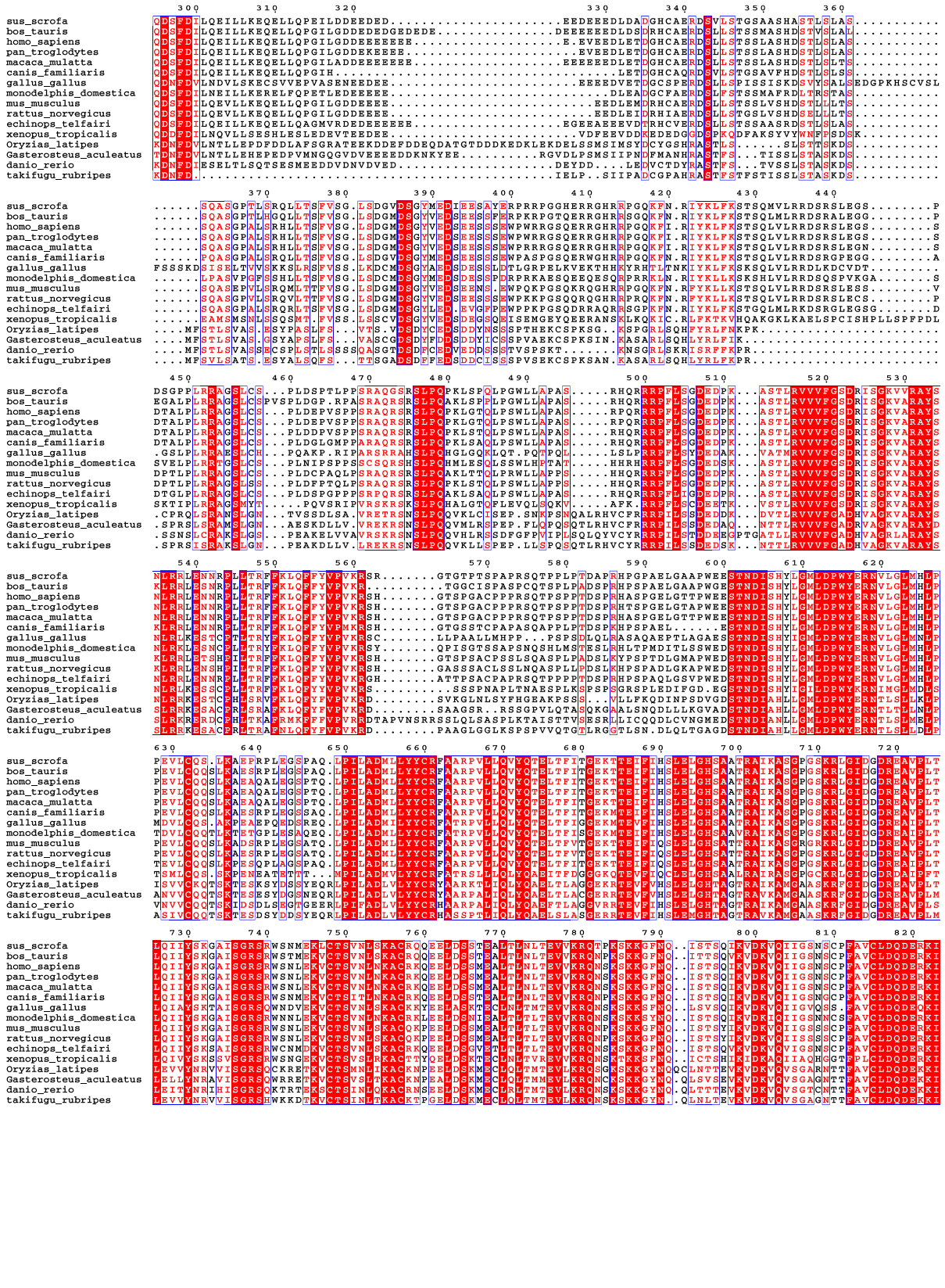
sus_scrofa
bos_tauris
homo_sapiens
pan_troglodytes
macaca_mulatta
canis_familiaris
gallus_gallus
monodelphis_domestica
mus_musculus
rattus_norvegicus
echinops_telfairi
xenopus_tropicalis
Oryzias_latipes
Gasterosteus_aculeatus
danio_rerio
takifugu_rubripes

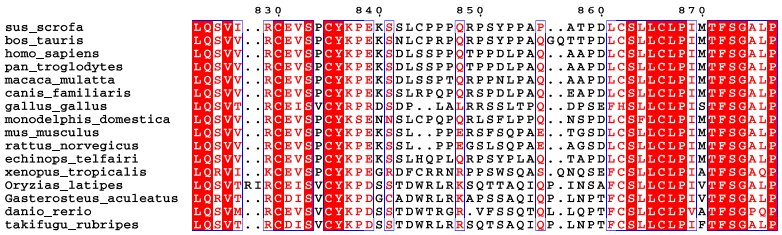

Figure 4.11: Alignment of p101 orthologues. The alignment was generated with the ClustalW algorithm and formatted with ESPript. Conserved and similar aa are highlighted by red boxes and red letters in blue boxes, respectively. Where available, sequence information was obtained from the Ensembl database (release 41). For *sus scrofa* (pig), the UniProt entry Y10472 was used. Protein entry codes for Ensembl entries: *homo sapiens* (human) ENSP00000369285, *pan troglodytes* (chimpanzee) ENSPTRP00000014908, *bos tauris* (cow) ENSBTAP00000007845, *macaca mulatta* (macaque) ENSMMUP00000007641, *canis familiaris* (dog) ENSCAFP00000025622, *gallus gallus* (chicken) ENSGALP00000001860, *monodelphis domestica* (opossum) ENSMODP00000010607, *mus musculus* (mouse) ENSMUSP00000021283, *rattus norvegicus* (rat) ENSRNOP00000030578, *echinops telfairi* (hedgehog) ENSETEP00000012315, *xenopus tropicalis* (xenopus) ENSXETP00000042245, *oryzias latipes* (medaka) ENSORLP00000003891, *gasterosteus aculeatus* (stickleback) ENSGACP00000025604, *danio rerio* (zebrafish) ENSDARP00000080053, *takifugu rubripes* (pufferfish) NEWSINFRUP00000149697.

Further information that may be obtained from the alignment lies in the exact boundaries of the domains and identification of functional NLS. Of the three motifs located by PSORTII (see section 4.1.1), only the one at position 499–502 (porcine numbering) appears to be largely conserved between species, indicating that only this one may be functionally relevant. At the N terminus, all but very few aa are identical or replaced in a conservative fashion. The first larger stretch of non-conserved aa appears at aa 183, possibly marking the C-terminal border of the interaction domain. Interestingly, the far N terminus shows a remarkable degree of conservation but seems to be expendable for interaction with p110γ. A still largely conserved stretch follows between aa 192–300. This region may constitute an extended binding surface for p110γ that increases the affinity between both proteins. In the C-terminal region of p101, a highly conserved stretch starts at aa 649, close to the mapped N-terminal border of the G$\beta\gamma$ binding domain. With the exception of a few divergent positions, all aa are identical or conserved up to aa 841, supposably marking the C-terminal end of the domain. Similar to the N terminus, the far C terminus is highly conserved, although it appears to be dispensable for binding to G$\beta\gamma$ or p110γ.

4.1.6 Data base mining for novel p110γ- and G$\beta\gamma$-binding proteins

The insight gained concerning the domain structure of p101, which is further supported by the localized similarity between the p101 orthologues (see Fig. 4.11), allowed to perform a focused search for novel p110γ-interacting and novel G$\beta\gamma$-interacting proteins. Aiming at identifying

novel G$\beta\gamma$ effectors, the C-terminal aa 650–850 of p101 were used as a BLAST search query against the translated, non-redundant nucleotide data base. Indeed, an mRNA sequence was identified that encodes a protein showing similarity to the C-terminal domain of p101 within its own C terminus (Fig. 4.12).

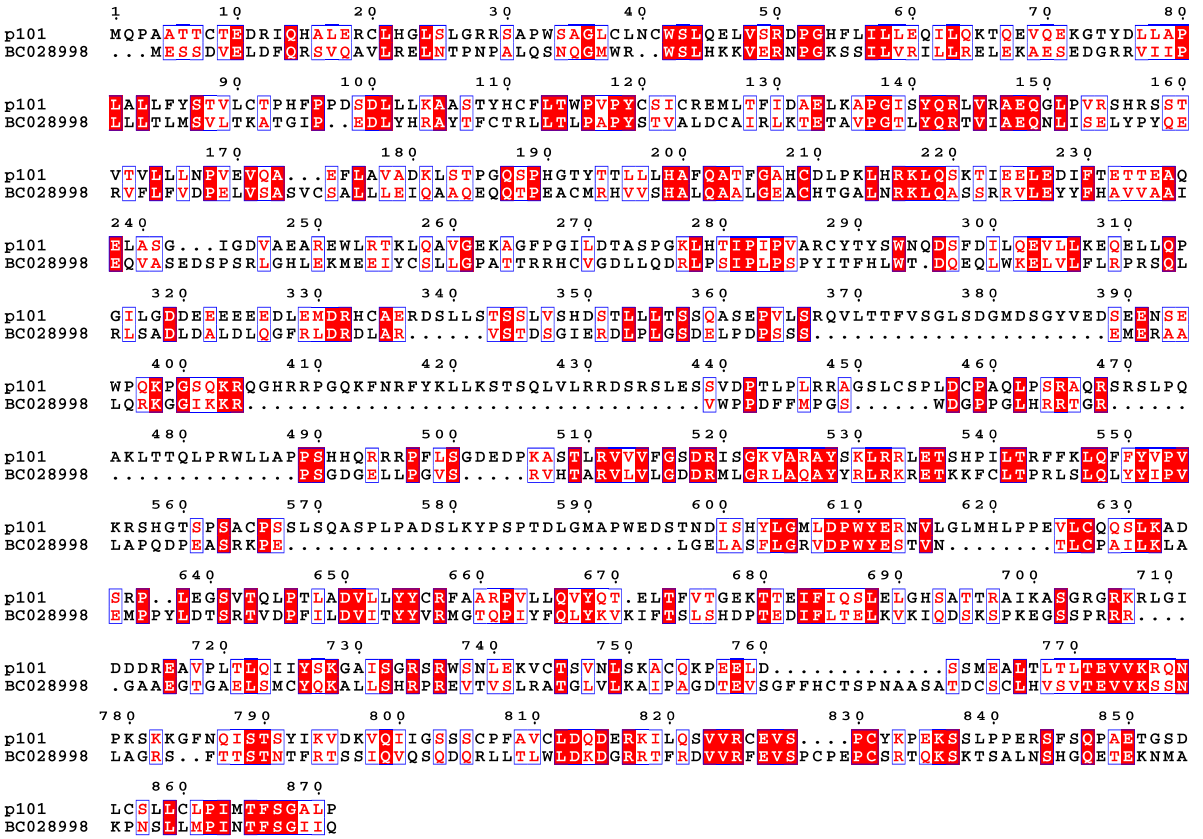

Figure 4.12: Alignment of murine p101 with a potential homologue. The alignment was generated with the ClustalW algorithm and was formatted with ESPript. Conserved and similar aa are highlighted by red boxes and red letters in blue boxes, respectively. The murine sequence of p101 (GenBank accession code NM_177320) was aligned with the transcript of the mRNA sequence BC028998 (GenBank accession code) identified by a BLAST search.

Surprisingly, closer inspection of the protein sequence revealed that the N terminus bears similarity to p101 as well, indicating that this protein may not only be a novel G$\beta\gamma$-interacting protein but may also bind p110γ. These features would allow this protein to act as a PI3Kγ regulatory subunit like p101. Although the overall conservation of 24% aa identity is lower as between the p101 orthologues, the regions corresponding to the interaction domains identified in p101 show a higher degree of conservation, best illustrated in a dot-plot presentation of the alignment (Fig. 4.13). Likewise, only a few short gaps with respect to p101 are present within the N and C terminus, whereas larger deletions are prominent within the middle part of the sequence. Hence, a functional relationship to p101 may exist. Moreover, expressed sequence tags (ESTs) corresponding to BC028998 were identified in a data base search. They originated

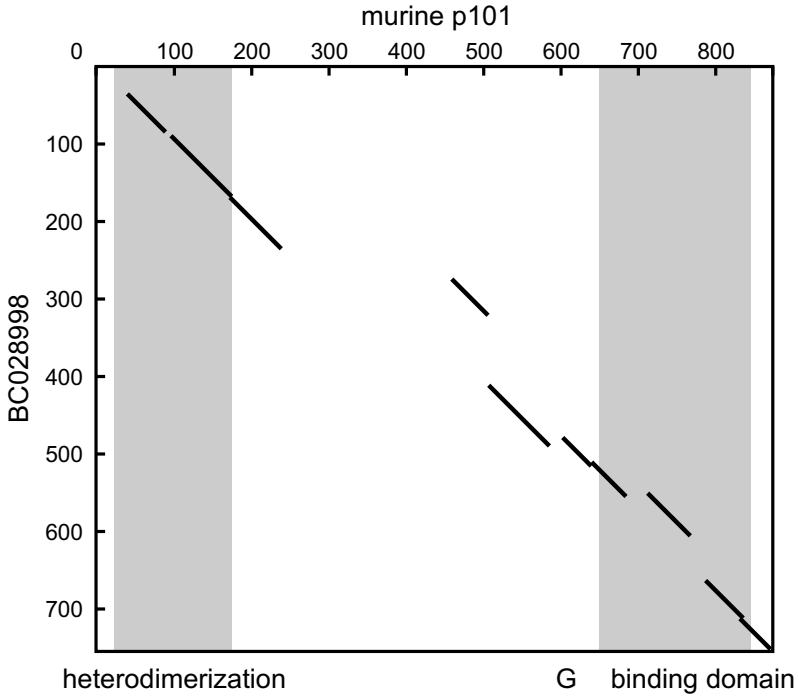

Figure 4.13: Dot-plot alignment of p101 with a potential p101 homologue. Bars indicate a minimum match of 28% identity over a window of 45 aa. The areas containing the interaction domains of p101 are shaded. The align was generated with MEGALIGN.

from tissues that are known to feature signaling pathways involving PI3Kγ and to express p110γ as well. Among them were constituents of the immune system such as bone marrow macrophages, DCs, lymph nodes, and thymus, as well as other organs such as heart and liver. Considering the striking similarity to p101 within its functional domains and the physiological evidence that the protein encoded by BC028998 may be expressed along with p110γ, it was investigated whether this protein may operate as a PI3Kγ regulatory subunit.

4.2 p87^{PIKAP} – a novel PI3Kγ regulatory subunit

The second part of this thesis deals with the cloning and characterization of p87^{PIKAP}, a novel regulatory subunit of PI3Kγ. The mRNA sequence that was identified based on the mapping of the functional domains within p101 (see section 4.1.6) indeed proved to encode a novel regulatory subunit of PI3Kγ. According to its function and molecular weight it was termed p87^{PIKAP}, PI3Kγ adapter protein of 87 kDa.

4.2.1 Cloning and basal characterization of p87^{PIKAP}

To examine its potential role of encoding a PI3Kγ regulatory subunit, it was first sought to clone the complete open reading frame of the identified mRNA sequence BC028998. Because several ESTs that were found for BC028998 originated from DCs, murine DCs were considered suitable for an RT-PCR-based cloning of the coding sequence. Using splenic CD11c$^+$ DCs and primers based on the sequence deposited in BC028998, the expected 2.3 kb fragment was readily obtained. The PCR product was subcloned, and several clones were sequenced. The obtained sequences were identical to the coding region of BC028998, with the exception of an in-frame 12-bp insert present in a few clones at the boundary of exons 12 and 13. Both sequences with and without the insert were submitted to the DDBJ/EMBL/GenBank data bases under the accession numbers AY753194 and DQ295832, respectively. Information from genome sequencing projects contained in the ENSEMBL data base allows the allocation of the p87^{PIKAP} gene to chromosome 11 in mice. It consists of 20 exons and is adjacent to the gene encoding p101 (see Fig. 5.2).

Initial studies using both short and long splice variants of p87^{PIKAP} did not result in any noticeable differences. Therefore, only data obtained for the short form will be presented here. Unlike p101, which accumulates in the nucleus when expressed alone, monomeric p87^{PIKAP} located to the cytosol of living HEK293 and COS-7 cells as assessed by confocal microscopy with YFP fusion proteins (Fig. 4.14, *upper panels*). The position of the fluorescent tag did not bear any observable influence on the localization pattern of p87^{PIKAP}. Coexpression of the catalytic p110γ subunit did not change the localization pattern of p87^{PIKAP} (Fig. 4.14, *lower panels*). This was in contrast to observations on p101. As already seen in HEK293 cells (see Fig. 4.1), YFP-p101 was located mostly within the cell nucleus in COS-7 cells and was excluded from the nucleus upon coexpression of p110γ (Fig. 4.14, *right panels*). In agreement with these results, analysis of the p87^{PIKAP} primary sequence with PSORTII (Nakai & Horton, 1999) did not reveal any NLS.

In previous studies it has been noted that p101 is rapidly degraded in the absence of p110γ (see for example Brock *et al.*, 2003). A reduced stability of p101 was already obvious in assessment of the subcellular localization, as the fluorescence intensity of YFP-p101 and p101-YFP was markedly lower if expressed without p110γ. To quantify this effect, cells were transfected

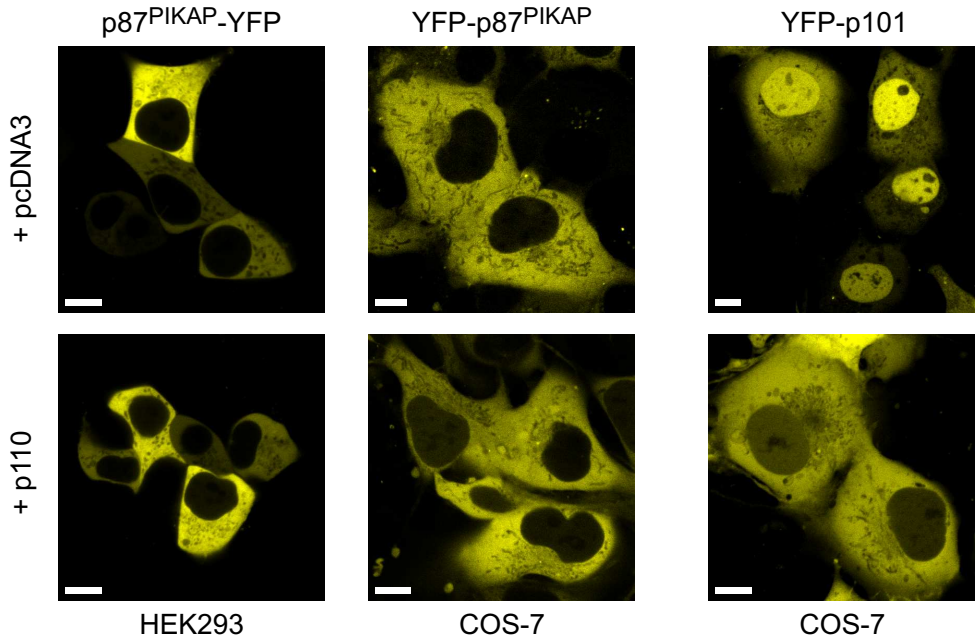

Figure 4.14: Subcellular localization of $p87^{PIKAP}$. HEK293 and COS-7 cells were transfected with plasmids encoding the indicated YFP fusions of $p87^{PIKAP}$ and p101 along with either pcDNA3 or p110γ. Cells were analyzed by confocal microscopy one day after transfection. Representative images are shown (bars: 10 μm).

with p101-YFP or $p87^{PIKAP}$-YFP and free CFP as a transfection marker. Two days after transfection, YFP fluorescence intensities were integrated over single cells that showed expression of CFP. If p101-YFP was expressed without p110γ, the background-corrected YFP fluorescence intensity was 36 $\pm$ 3% of the level observable for coexpression of p110γ (75–120 cells each, three experiments). However, such a pronounced effect was not visible for $p87^{PIKAP}$. Withdrawal of p110γ decreased fluorescence intensities of $p87^{PIKAP}$-YFP-transfected cells only slightly to 75 $\pm$ 2% of the value obtained on cells that coexpress p110γ. To extend these findings, HEK293 cells were transfected with varying amounts of FLAG-tagged regulatory and catalytic subunit, and their expression was assessed in whole cell lysates by Western blot. If both subunits do not rely on each other for a stable expression, reduction of the amount of plasmid transfected for one subunit should not influence the expression of the other. Such a behavior was observed for p110γ-FLAG and $p87^{PIKAP}$-FLAG. Expression of both subunits correlated only with the amount of plasmid transfected (Fig. 4.15, *lower panel*). However, expression of p101 was clearly reduced if less p110γ was present (Fig. 4.15, *upper panel*). Accordingly, p101 appears to be stabilized by coexpression of p110γ, whereas $p87^{PIKAP}$ is more stable even if p110γ is absent.

4.2.2 Interaction of $p87^{PIKAP}$ with p110γ

To demonstrate an interaction of $p87^{PIKAP}$ with p110γ, co-IP experiments were performed. CFP-p101, which was employed as a positive control, was detectable in immunoprecipitates

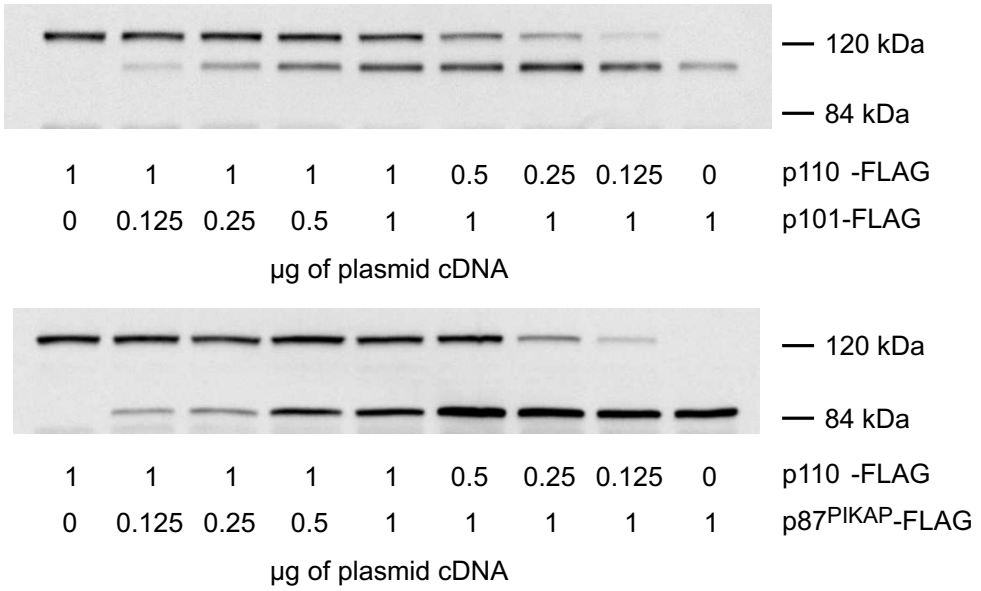

Figure 4.15: Stability of p87^{PIKAP} and p101 . HEK293 cells were transfected with varying amounts of the indicated plasmids encoding FLAG-tagged p110γ and p101 (upper panel) or p87^{PIKAP} (lower panel). The total amount of transfected plasmid DNA (2 μg) was kept constant by addition of pcDNA3 where necessary. Two days after transfection, whole cell lysates were prepared and analyzed by SDS-PAGE and immunoblot with an anti-FLAG antibody.

generated by precipitation of p110γ-FLAG from lysates of HEK293 cells that were transfected with p110γ-FLAG and CFP-p101 (Fig. 4.16). Likewise, CFP-p87^{PIKAP} was readily copurified with p110γ-FLAG, whereas a CFP-YFP fusion protein, which was used to control for unspecific binding due to the CFP moiety, was not present in the immunoprecipitate. Thus, p87^{PIKAP} indeed forms a complex with p110γ.

The interaction was further characterized by the use of FRET. A representative measurement of CFP-p87^{PIKAP} and YFP-p110γ in living HEK293 cells is shown in Fig. 4.17*A,B*. A FRET efficiency of about 17% was obtained. To test whether this efficiency reflects a specific interaction, FRET competition assays were performed. If FRET between two fluorescent fusion proteins is the result of a specific interaction, coexpression of one of the interacting partners in untagged form is expected to displace the tagged variant from its interaction partner, leading to a concomitant reduction in the overall FRET efficiency. For CFP-p87^{PIKAP} and YFP-p110γ, coexpression of either untagged p87^{PIKAP} and p110γ led to a concentration-dependent decrease in FRET efficiencies (Fig. 4.17*C,D*), confirming that the measured FRET signals arise from a specific interaction. Furthermore, negligible energy transfer occured if CFP-p87^{PIKAP} and YFP-p87^{PIKAP} were coxpressed with free YFP and CFP, respectively (Fig. 4.17*E,F*). Similarly, very low FRET efficiencies were obtained if p110γ fusion proteins were replaced by YFP-p110β or p110β-YFP (Fig. 4.17*E,F*), supporting the concept that p87^{PIKAP} is a class IB PI3K adapter protein that does not interact with class IA PI3K catalytic subunits.

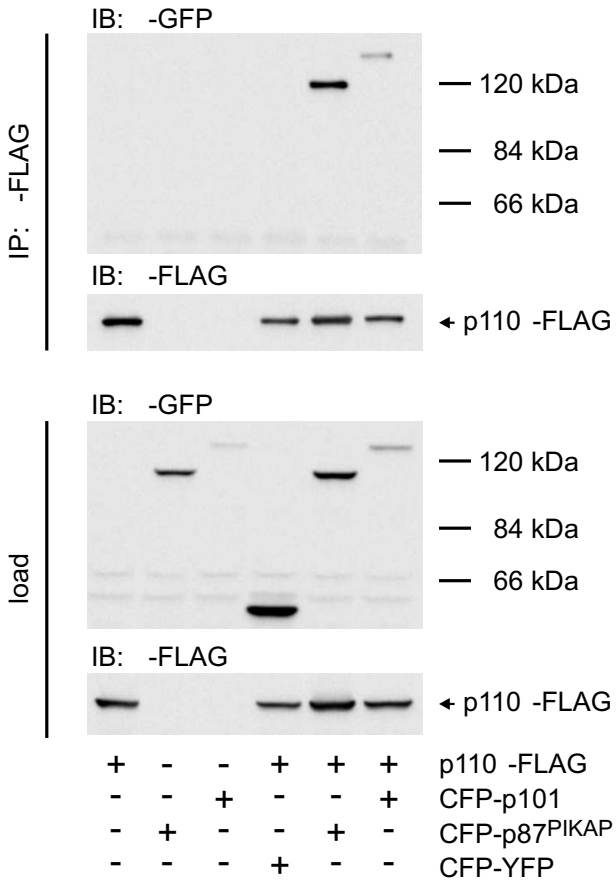

Figure 4.16: Coimmunoprecipitation of $p87^{PIKAP}$ and p110γ-FLAG. HEK293 cells were transfected with plasmids encoding p110γ-FLAG and CFP-tagged regulatory PI3K subunits. p110γ-FLAG was immunoprecipitated from cleared lysates with an anti-FLAG antibody. Immunoprecipitates were assayed for the presence of regulatory subunits by immunoblotting with an anti-GFP antibody (IP). Lysates were probed with the same antibodies to verify expression of the subunits (load).

To explore the spatial relations within the p110γ/$p87^{PIKAP}$ dimer, FRET efficiencies were determined for all combinations of N- and C-terminally tagged $p87^{PIKAP}$ and p110γ. Regardless of the donor–acceptor assignment, higher FRET efficiencies were obtained if the fluorescent proteins were located at the same termini in $p87^{PIKAP}$ and p110γ (Fig. 4.17*E,F*). As FRET efficiencies correlate to distances given that the rotation of the fluorescent moieties is unhindered, each the N and C termini of $p87^{PIKAP}$ and p110γ are closer to each other than to the opposite termini. A similar situation has been observed for p101 and p110γ (Brock *et al.*, 2003), indicating that the relative orientations of the proteins in the p110γ/p101 and p110γ/$p87^{PIKAP}$ complexes are probably very similar.

The FRET efficiency between CFP-$p87^{PIKAP}$ and YFP-p110γ was considerably higher than that between CFP-p101 and YFP-p110γ (see Fig. 4.2). Given that p101 binds tightly and almost quantitatively to p110γ (see for example Stephens *et al.*, 1997; Brock *et al.*, 2003), it is unlikely that the higher FRET efficiency directly translates to a higher affinity of $p87^{PIKAP}$ for p110γ. It may rather reflect either shorter distances between the CFP and YFP moieties of the fusion proteins – probably also due to variations in the linker sequences – or locally different conformations at the N and C termini in each complex. To nevertheless investigate the relative p110γ binding properties of p101 and $p87^{PIKAP}$, additional FRET competition assays were performed.

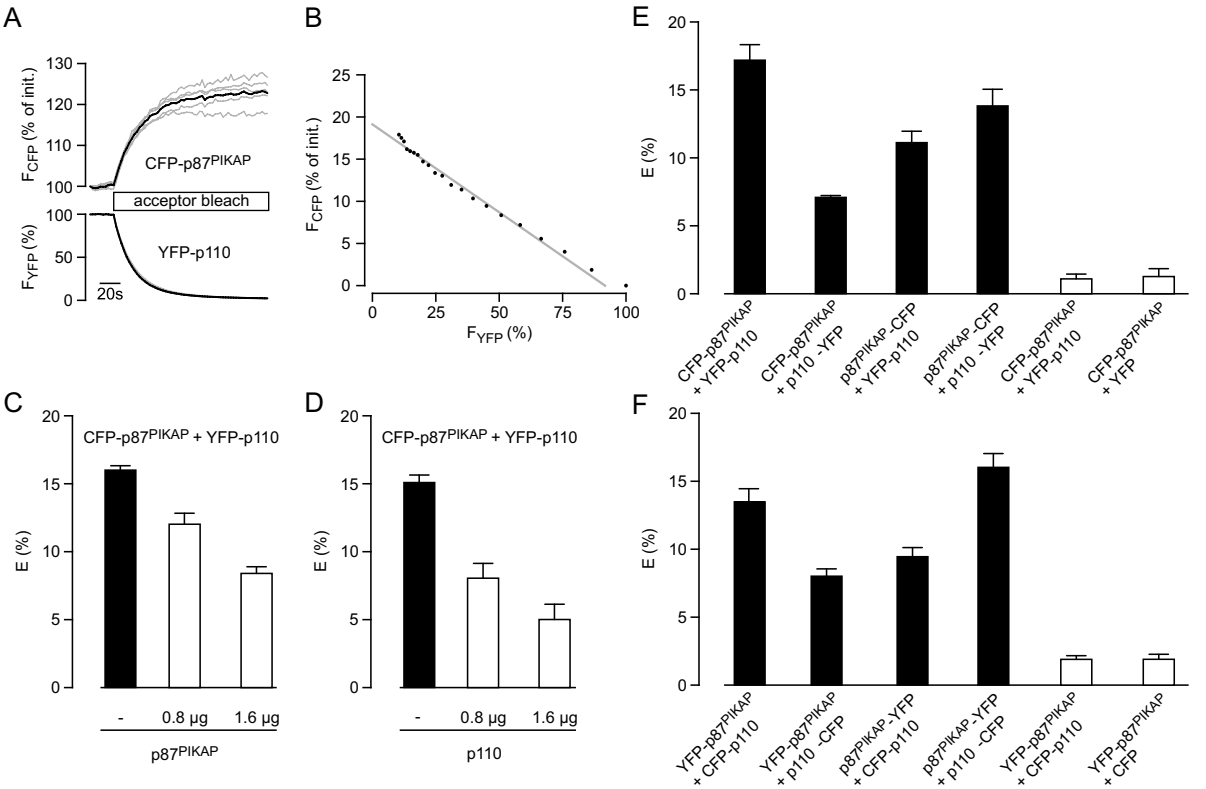

Figure 4.17: FRET between fluorescent fusion proteins of p110γ and p87^{PIKAP}. FRET was measured in living HEK293 cells transfected with plasmids encoding the indicated fluorescent fusion proteins. *A*, single cell (gray lines) and mean (black lines) fluorescence traces of CFP and YFP obtained during a representative acceptor photobleach measurement of cells expressing CFP-p87^{PIKAP} and YFP-p110γ. *B*, regression analysis of donor recovery during YFP photobleach based on the mean traces of the experiment shown in *A*. In this way, the CFP recovery at complete YFP photobleach was extrapolated to calculate the FRET efficiency with the formula given in section 3.6.3. *C and D*, FRET competition assays. If FRET originates from a specific interaction between fusion proteins, the FRET efficiency will be reduced upon coexpression of untagged wild-type proteins. The indicated amounts of plasmids encoding untagged p87^{PIKAP} (*C*) or p110γ (*D*) were transfected along with constant amounts of plasmids encoding YFP-p110γ and CFP-p87^{PIKAP}. *E,F*, FRET efficiencies for the indicated combinations of N- and C-terminally CFP- and YFP-tagged p87^{PIKAP} and p110γ. CFP was fused to either p87^{PIKAP} (*E*) or p110γ (*F*). Combinations with free fluorescent proteins and p110β were employed as controls. For all data shown in *C–F*, means and S.E. of four independent measurements with at least six cells each are shown.

Here, the interaction between one of the regulatory subunits and p110γ-YFP was perturbed by coexpression of p101, p87^{PIKAP}, or p85α. As expected, p101-CFP was displaced from binding to p110γ by both p101 and p87^{PIKAP}, whereas the class IA regulatory subunit p85α was ineffective in lowering the FRET efficiency (Fig. 4.18*A*). Comparable data were obtained for competition of the interaction between p110γ-YFP and p87^{PIKAP}-CFP (Fig. 4.18*B*). Thus, p101 and p87^{PIKAP} bind to p110γ in a mutually exclusive fashion at identical or overlapping binding sites. Because both p101 and p87^{PIKAP} are similarly efficient in displacing each other from p110γ, it may be

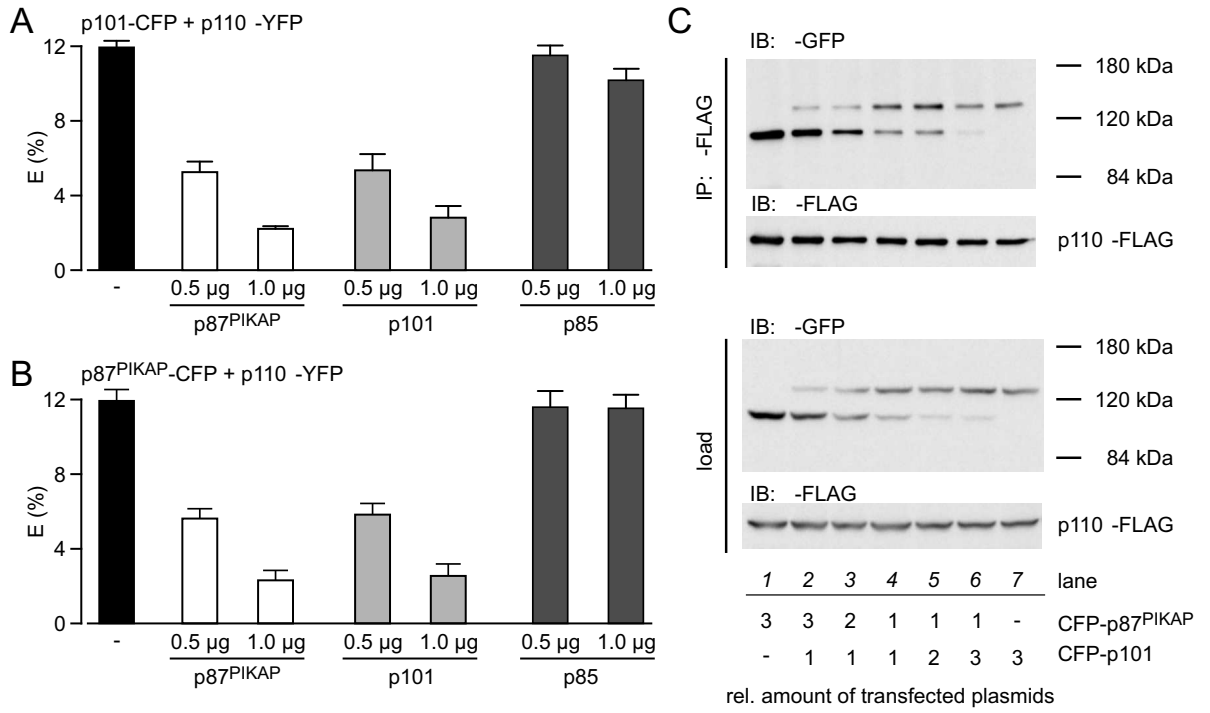

Figure 4.18: Competition of FRET between PI3Kγ subunits and competitive coimmunoprecipitation of $p87^{PIKAP}$ and p101 with p110γ. *A,B*, FRET was measured in living HEK293 cells transfected with plasmids encoding p110γ-YFP and either p101-CFP (*A*) or $p87^{PIKAP}$-CFP (*B*). To displace binding of the fluorescent regulatory subunits, vectors encoding wild-type untagged $p87^{PIKAP}$, p101, or p85α were cotransfected in different amounts. Empty vector (pcDNA3) was used to keep the amount of transfected plasmid constant. Means and S.E. of four independent measurements with at least six cells each are shown. *C*, HEK293 cells were transfected with plasmids coding for p110γ-FLAG and CFP-tagged p101 and $p87^{PIKAP}$. p110γ-FLAG was immunoprecipitated with an anti-FLAG antibody, and the extent of copurification of regulatory subunits was assessed by immunoblot with an anti-GFP antibody (IP). Lysates were checked for expression of p110γ-FLAG and regulatory subunits with the same antibodies (load). The blots shown are representative for a set of three experiments.

argued that both proteins share comparable affinity for p110γ.

For a more direct assessment of their relative affinities towards p110γ, copurification of CFP-tagged p101 and $p87^{PIKAP}$ was examined in a competitive setting. To this end, variable amounts of regulatory subunits were coexpressed along with a constant and limiting amount of p110γ in HEK293 cells. p110γ-FLAG was immunoprecipitated, and the extent of copurification of the CFP-tagged regulatory subunits was assessed and compared to the levels found in the cell lysates. If comparable quantities of CFP-p101 and CFP-$p87^{PIKAP}$ were present in the lysates, a slight but discernible excess of CFP-$p87^{PIKAP}$ was detected in the immunoprecipitate (Fig. 4.18*C, lane 3*). If expression of CFP-p101 was slightly higher, CFP-$p87^{PIKAP}$ still displayed a more efficient copurification (Fig. 4.18*C, lanes 4 and 5*). Still, if even more CFP-p101 was expressed, CFP-$p87^{PIKAP}$ was almost completely displaced (Fig. 4.18*C, lane 6*). Taken together,

the affinity of p87^{PIKAP} towards p110γ may slightly exceed that of p101.

4.2.3 Interaction of p87^{PIKAP} with G$\beta\gamma$

The function of a PI3Kγ regulatory subunit is crucially dependent on its ability to bind to G$\beta\gamma$, the activating principle of PI3Kγ signaling. Therefore, the interaction of p87^{PIKAP} with G$\beta\gamma$ was analyzed. First, it was attempted to probe the interaction *via* an recruitment assay equal to that performed in the characterization of the G$\beta\gamma$ binding site of p101 (see for example Fig. 4.2). However, it was not possible to detect a membrane localization of p87^{PIKAP} upon coexpression of p87^{PIKAP}-YFP or YFP-p87^{PIKAP} with G$\beta_1\gamma_2$, whereas a recruitment to the plasma membrane was discernible for p101-YFP under the same conditions (data not shown). These findings may indicate a lower affinity of p87^{PIKAP} for G$\beta\gamma$. To both enhance the sensitivity of detection and to test whether the affinity of p87^{PIKAP} towards G$\beta\gamma$ is still sufficient to ensure activation of p110γ, the catalytic activity of p110γ was utilized, and an assay based on PI3Kγ activity was set up. The YFP-Grp1-PH construct allows to easily measure the activity of class I PI3Ks by monitoring its subcellular localization. In HEK293 cells transfected with G$\beta\gamma$, YFP-Grp1-PH was almost exclusively located within the cytosol, indicating the absence of appreciable PI3K activity (Fig. 4.19*A, left panels*). Membrane localization of a minor fraction of YFP-Grp1-PH was observed upon expression of p110γ along with G$\beta\gamma$, pointing to the presence of marginal PI3K activity. A pronounced membrane localization that indicates a high and persistent activity of PI3Kγ, however, was only achieved if either p101 or p87^{PIKAP} were present as well (Fig. 4.19*A, middle panels*). Thus, p87^{PIKAP} as well as p101 bind to G$\beta\gamma$ in this context, thereby acting as PI3Kγ regulatory subunits and enabling activation of p110γ. In line with the absence of a distinct membrane localization of p87^{PIKAP} upon coexpression of G$\beta\gamma$, the extent of activation was slightly lower if p87^{PIKAP} was present instead of p101. Accordingly, p101 may indeed have a higher affinity for G$\beta\gamma$ than has p87^{PIKAP}.

Membrane localization of YFP-Grp1-PH was strongly attenuated upon coexpression of the G$\beta\gamma$-scavenging C terminus of the β-adrenergic receptor kinase (βARK-CT-CFP; Fig. 4.19*A, right panel*). Moreover, YFP-Grp1-PH was confined to the cytosol upon omission of G$\beta\gamma$. Both observations indicate that G$\beta\gamma$ is essential for the p87^{PIKAP}-mediated activation of p110γ. Catalytic activity of p110γ was mandatory for membrane localization of YFP-Grp1-PH, as shown by the use of a catalytically inactive mutant of p110γ (Fig. 4.19*A, right panel*). Comparable results were obtained if the phosphorylation state of Akt was analyzed. Akt is a central component of PI3K signaling and among the primary effectors immediately downstream of the class I PI3Ks. A pronounced activation of Akt was only observed if either p87^{PIKAP} or p101 were present (Fig. 4.19*B*).

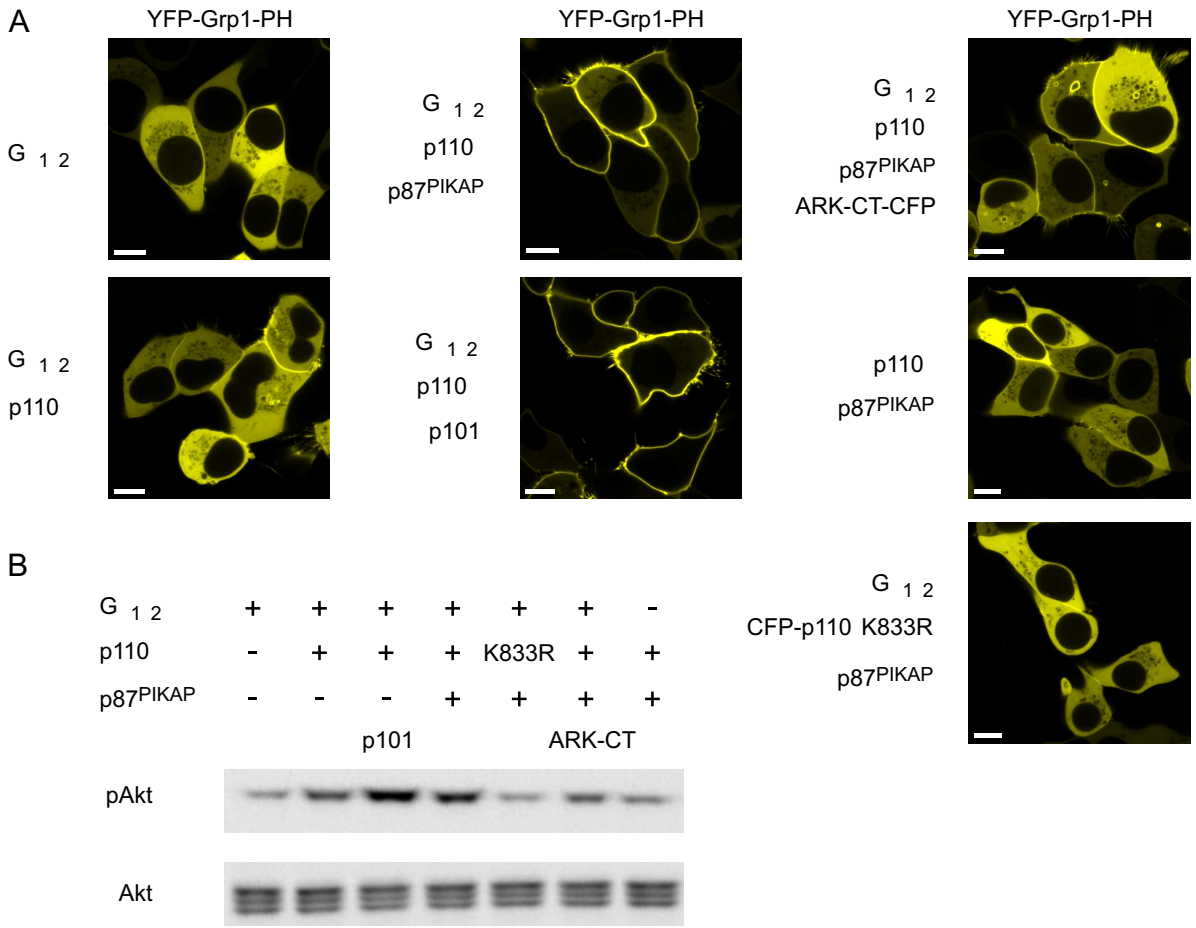

Figure 4.19: Activation of PI3Kγ reveals interaction between $p87^{PIKAP}$ and G$\beta\gamma$. *A*, the subcellular localization of the translocating PI3K biosensor YFP-Grp1-PH is shown for HEK293 cells transfected with plasmids encoding YFP-Grp1-PH, Gβ_1, Gγ_2, p110γ, p101, and $p87^{PIKAP}$ in the combinations stated in the figure. Images were obtained by confocal microscopy. Representative images from at least three independent experiments are shown (bars: 10 μm). *B*, the phosphorylation of Akt at Ser 473 was monitored in HEK293 cells transfected as in *A* but without YFP-Grp1-PH. Whole cell lysates were probed with an anti-phospho-Akt (Ser^{473}) as well as with an anti-Akt antibody to show equal loading. Note that all three isoforms of Akt are recognized by the anti-Akt antibody.

4.2.4 Reconstitution of PI3Kγ signaling

To translate the findings obtained for the static overexpression of G$\beta\gamma$ to the dynamic situation found in living cells after GPCR stimulation, a PI3Kγ signaling pathway was reconstituted in HEK293 cells. To this end, cells were transfected with the human fMLP receptor and various combinations of PI3Kγ subunits. Activation of PI3Kγ was assessed by monitoring the translocation of YFP-Grp1-PH. Stimulation with 1 µM fMLP did not result in a discernible membrane translocation in cells transfected only with the fMLP receptor and p110γ (Fig. 4.20*A*). In agreement with the data shown in Fig. 4.19, expression of either p101 or $p87^{PIKAP}$ was mandatory for

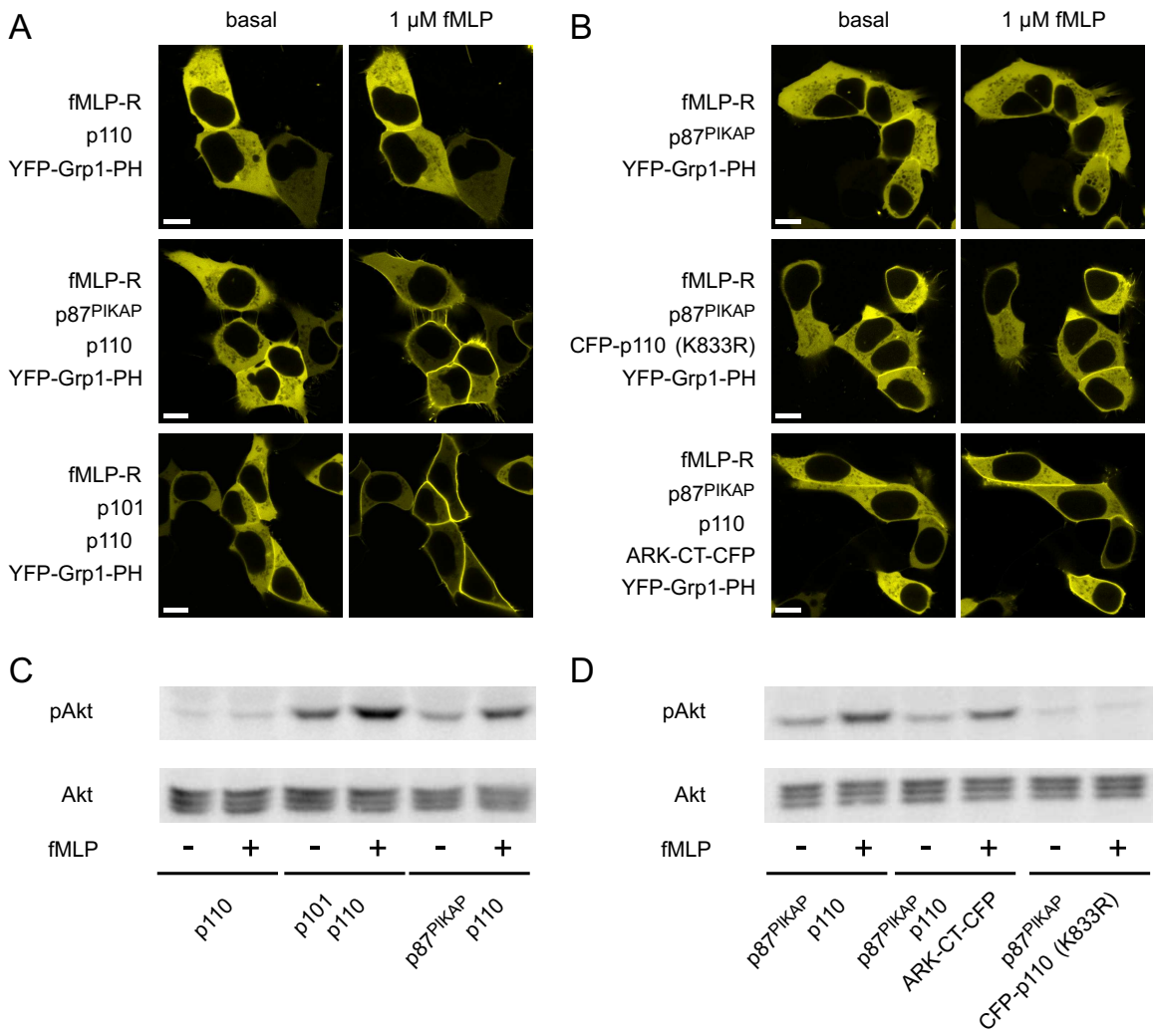

Figure 4.20: p87^{PIKAP}mediates activation of PI3Kγ downstream of GPCR stimulation. *A,B*, membrane recruitment of YFP-Grp1-PH was assayed by confocal microscopy upon stimulation with 1 μM fMLP. HEK293 cells were transfected with plasmids encoding YFP-Grp1-PH, the fMLP receptor, p110γ, p101, and p87^{PIKAP} in the combinations indicated in the figure. Images were taken before and 2 min after addition of fMLP (bars: 10 μm). They are representative of at least three independent experiments each. *C,D*, analysis of Akt phosphorylation. HEK293 cells were transfected with the indicated plasmids. Whole cell lysates were probed for total Akt and phosphorylated Akt (Ser^{473}) by immunoblot analysis with the respective antibodies.

activation of PI3Kγ, as reflected by a marked translocation of YFP-Grp1-PH (Fig. 4.20*A*). Again, a more pronounced translocation was mediated by the p101-containing PI3Kγ heterodimer. The translocation of YFP-Grp1-PH was abolished if either a catalytically inactive p110γ was expressed or if p110γ was omitted (Fig. 4.20*B*, data not shown for p101). Both the p101- and p87^{PIKAP}-mediated activation were dependent on the accessibility of G$\beta\gamma$ complexes released from heterotrimeric G proteins upon GPCR stimulation, because coexpression of βARK-CT significantly reduced the translocation of YFP-Grp1-PH (Fig. 4.20*B*, data not shown for p101).

Very similar results were obtained in the examination of Akt phosphorylation upon fMLP stimulation (Fig. 4.20*C,D*). Thus, p87^{PIKAP} is able to mediate the activation of p110γ upon GPCR stimulation in the same way as p101.

4.2.5 Expression pattern of p87^{PIKAP}

After having shown that p87^{PIKAP} meets all requirements for a PI3Kγ regulatory subunit, its expression pattern was assessed to explore in which physiological setting p87^{PIKAP} may be of special importance to PI3Kγ signaling. First, the expression of p87^{PIKAP} mRNA was investigated by Northern blot analysis.

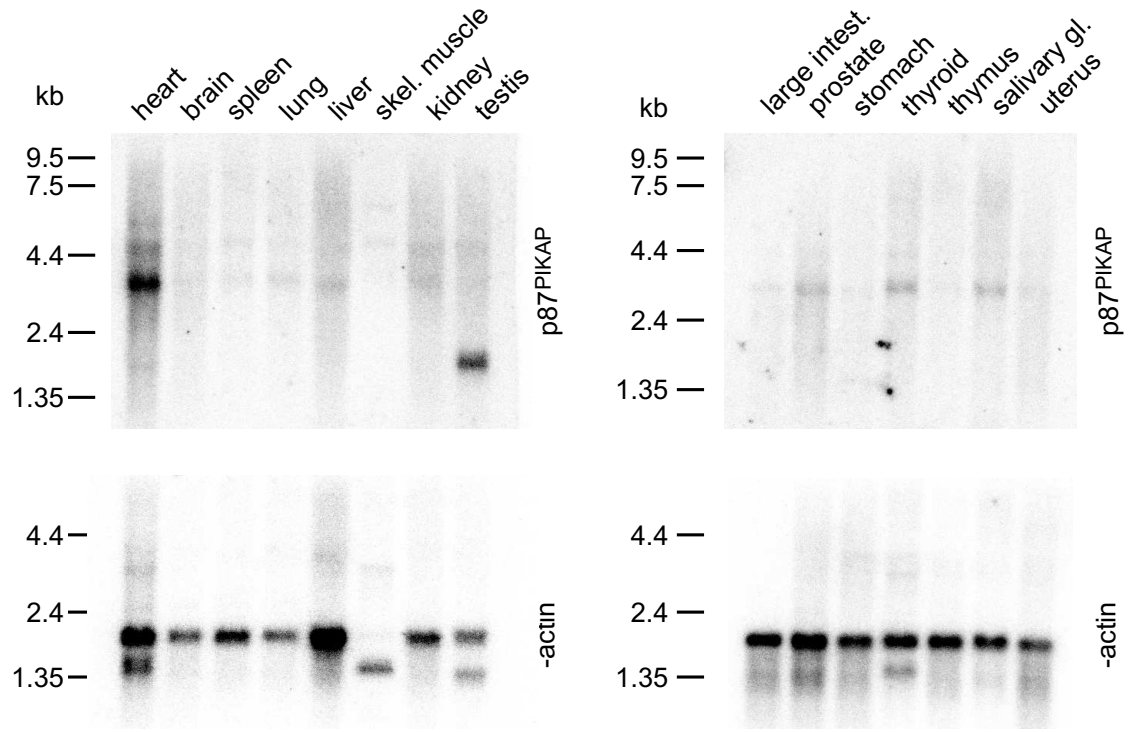

Figure 4.21: Northern blot analysis of p87^{PIKAP} expression. Premade Northern blots containing 2 μg poly(A$^+$) RNA isolated from multiple tissues of 8–10-week-old mice were hybridized with a p87^{PIKAP} probe spanning bases 1624–2259 of the coding sequence. Equal loading was controlled by hybridization of the same blots with a β-actin control probe.

The expected 3.2-kb transcript was detected in several tissues including brain, spleen, lung, liver, kidney, prostate, thyroid, and salivary glands, indicating that p87^{PIKAP} is broadly expressed (Fig. 4.21). The strongest signal, however, was obtained in heart. A shorter transcript was present in testis. Because it is too short to encode full-length p87^{PIKAP}, it was not investigated further. It may represent a substantially shorter splice variant that therefore presumably lacks functionally important elements. Surprisingly, the message was barely detectable in thymus, although PI3Kγ is involved in many physiological aspects of leukocytes. It is possible that

the adult age of the mice precluded detection in thymus, because this organ degenerates with age. EST data bases (see UniGene entry Mm.234573) yielded entries corresponding to p87^{PIKAP} in thymus, DCs, and bone marrow macrophages, indicating that p87^{PIKAP} may still be relevant to PI3Kγ signaling in leukocytes. Moreover, EST data corroborate the findings of the Northern blots for most tissues, and further reveal expression in aorta.

To obtain an indication concerning the relative contributions of p101 and p87^{PIKAP} to PI3Kγ signaling, the expression of all three PI3Kγ subunits was analyzed by multiplex PCR assays on reverse-transcribed RNA from heart, spleen, thymus, and different subsets of leukocytes. These cell types were chosen because they have all been shown to harbor physiologically important PI3Kγ signaling cascades. As expected, expression of p110γ was detectable in all cell types assayed, albeit to variable extent (Fig. 4.22*A*). In agreement with the Northern blot data, p87^{PIKAP} was highly expressed in heart. Interestingly, expression of p101 was markedly lower in heart. On the other hand, spleen and thymus showed pronounced signals for p101 but not for p87^{PIKAP} expression, again in agreement with the Northern blot (see Fig. 4.21). Still, a closer examination of leukocyte subspecies revealed that p87^{PIKAP} is expressed along with p101 in several types of leukocytes. Whereas p101 was the only regulatory subunit detectable in B and T cells, p87^{PIKAP} was present in macrophages, neutrophils, and various subtypes of DCs (Fig. 4.22*A*).

As p101 and p87^{PIKAP} are simultaneously expressed within the same cell type but bear different properties *e.g.* concerning their interaction with G$\beta\gamma$, the relative amount of expression may influence the signaling events mediated by PI3Kγ. Thus, in order to obtain more quantitative information about the relative expression levels of p101 and p87^{PIKAP}, competitive PCRs were performed. In a competitive PCR, an internal standard is amplified together with the fragment of interest in the same reaction using the same primers, thereby providing identical conditions for the amplification of both fragments. To generate an internal standard that is as similar to the cDNA to quantify as possible, a template construct was generated each for p101 and p87^{PIKAP} that was identical to the fragment amplified in the multiplex PCRs except for a 40-bp deletion following the forward primer binding site. The number of template molecules for the internal standard was varied to find conditions where amplification of the cDNA fragment and the internal standard was equally efficient. Then, about equal amounts of template for both fragments should have been present in the reaction. Panels of competitive PCRs were performed with cDNA prepared from heart, neutrophils, and CD11b^{+} DCs, which all contain different ratios of p101 and p87^{PIKAP}. In heart, p87^{PIKAP} mRNA is about 5 times more abundant than mRNA encoding p101, amounting to ~21,500 and ~4,400 copies for p87^{PIKAP} and p101, respectively, per 100 ng of total RNA (Fig. 4.22*B, upper panel*). In neutrophils, copies of p87^{PIKAP} mRNA were fewer than those of p101 mRNA (~37,900 copies and ~107,000 copies, respectively, per ng of poly(A^{+}) RNA; Fig. 4.22*B, middle panel*). In DCs, the excess of p101 was even more pronounced, yielding ~30,800 and ~120,000 copies of p87^{PIKAP} and p101 mRNA,

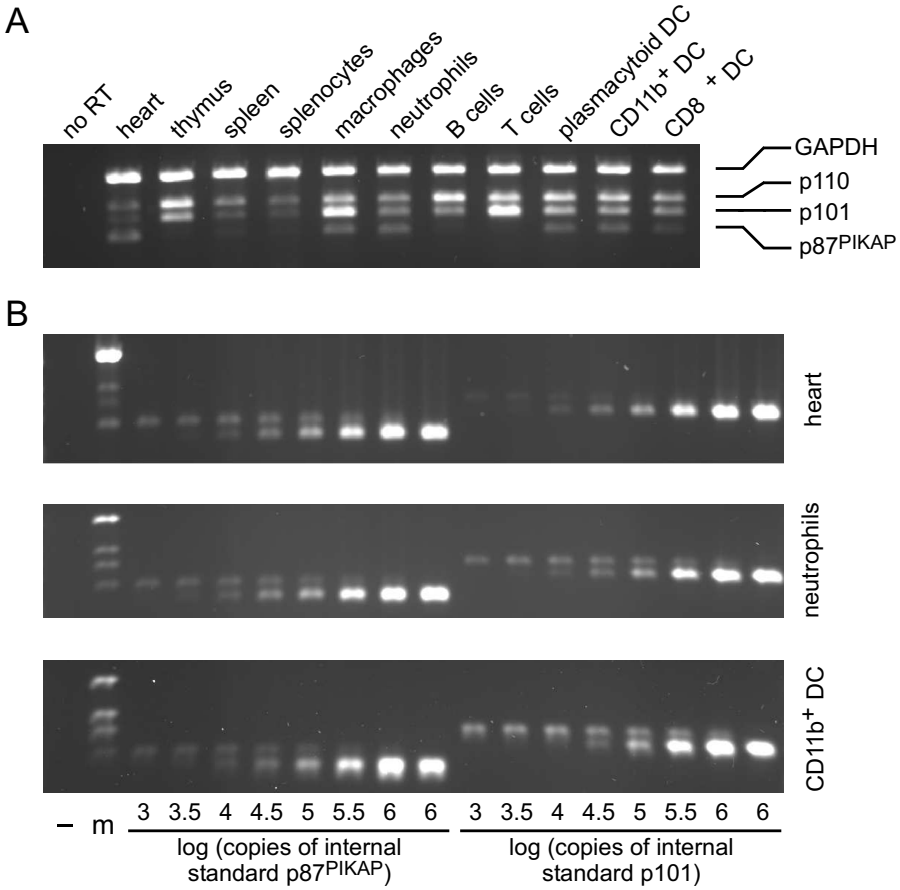

Figure 4.22: Multiplex PCR analysis of the relative expression levels of PI3Kγ subunits in various cell types. *A*, fragments of GAPDH, p110γ, p101, and $p87^{PIKAP}$ cDNA were simultaneously amplified by multiplex PCR on reverse-transcribed RNA from different leukocyte subsets and heart. The number of cycles was limited to 24, which was shown to yield template-limited amounts of PCR products in preceding preliminary assays. *B*, competitive PCRs were performed to assess the relative expression of p101 and $p87^{PIKAP}$ in selected cell types. Constant amounts of cDNA were offered as template in each PCR, while the number of template molecules of the internal standard was varied from 10^3–10^6 as indicated below. In reactions yielding equal amounts of product for the cDNA and the internal standard fragment, an equal number of template molecules had been present for both fragments. Further lanes contained PCRs with neither reverse-transcribed RNA nor internal standard (–), only internal standard (last lane of each set for $p87^{PIKAP}$ and p101), or with conditions identical to those shown in *A* (m). *A,B*, ethidium bromide-stained agarose gels of PCRs representative of three experiments each are shown.

respectively, per 100 ng of total RNA (Fig. 4.22*B, lower panel*). Taken together, it is likely that signaling *via* PI3Kγ relies almost exclusively on $p87^{PIKAP}$ in heart, whereas other cell types that express $p87^{PIKAP}$ do so only in combination with p101.

To establish functions specific for $p87^{PIKAP}$, it is advisable to focus on cells that express $p87^{PIKAP}$ as the only regulatory subunit of PI3Kγ. In searching for a suitable cell culture model to study the function of $p87^{PIKAP}$ by knockdown experiments, the rat basophilic leukemia cell

line RBL-2H3 was found to contain only p87^{PIKAP} but not p101 mRNA, extending the panel of p87^{PIKAP}-expressing leukocytes (see section 4.2.7). Therefore, further analysis to elucidate the cellular function of p87^{PIKAP} focused on both heart and RBL-2H3 cells.

4.2.6 Interaction of p87^{PIKAP} with PDE3B

The role of PI3Kγ in the regulation of myocardial contractility and in cardiac remodeling processes has been discovered in the characterization of p110γ knockout mice (Crackower *et al.*, 2002). Recent studies have shown that both effects are mediated by different properties of p110γ. While the pathways involved in remodeling are dependent on catalytic activity of p110γ, the impact on contractility is likely conveyed by a scaffolding interaction with PDE3B, resulting in activation of PDE3B (Patrucco *et al.*, 2004). However, the interaction is probably mediated by additional proteins, as recombinant p110γ did not activate PDE3B in PDE3B-directed immunoprecipitates derived from hearts of p110γ knockout mice (Patrucco *et al.*, 2004). Considering the strong expression of p87^{PIKAP} in heart (see Fig. 4.21 and 4.22), it was explored whether p87^{PIKAP} may connect p110γ with PDE3B.

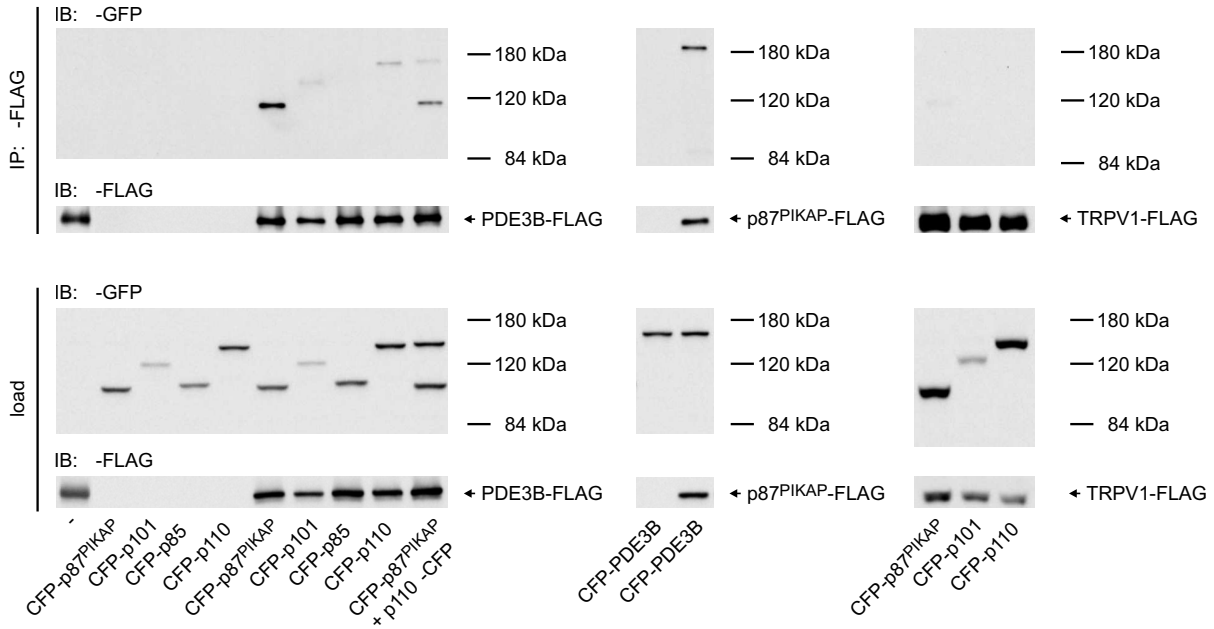

Figure 4.23: Interaction of p87^{PIKAP} with PDE3B. HEK293 cells were transfected with plasmids encoding the indicated FLAG- and CFP-tagged proteins. FLAG-tagged proteins were immunoprecipitated from cell lysates with an anti-FLAG antibody. The recovery of FLAG-tagged protein was analyzed with an anti-FLAG antibody, and copurification of CFP-tagged proteins was assessed with an anti-GFP antibody (IP). Lysates were probed with the same antibodies to verify expression (load). *Left panel*, IP of PDE3B-FLAG, *middle panel*, IP of p87^{PIKAP}-FLAG, *right panel*, IP of TRPV1-FLAG used as a negative control. The IP experiments shown are representative of three each.

To this end, HEK293 cells were transfected with various combinations of PDE3B-FLAG and

CFP-tagged PI3K subunits. Efficient copurification was observed for CFP-$p87^{PIKAP}$, whereas only weak signals were obtained for CFP-p101 and CFP-p110γ (Fig. 4.23, *left panel*). CFP-p85α, which was used as a control, was not copurified. Likewise, all PI3K subunits were absent from immunoprecipitates if PDE3B-FLAG was omitted. *Vice versa*, copurification of CFP-PDE3B was readily detectable upon IP of $p87^{PIKAP}$-FLAG (Fig. 4.23, *middle panel*). As an additional control, cells were transfected with TRPV1-FLAG instead of PDE3B-FLAG. Under these conditions, signals were barely detectable or absent for the CFP-tagged PI3Kγ subunits in the anti-FLAG immunoprecipitates (Fig. 4.23, *right panel*). All combinations shown in Fig. 4.23 were repeated with a modified IP protocol employing a RIPA buffer, giving rise to very similar results (data not shown). Moreover, to further exclude lysis artifacts, HEK293 cells were separately transfected with PDE3B-FLAG, $p87^{PIKAP}$, p101, or p110γ. The lysates derived from these cells were combined and subjected to the IP procedure. Under these conditions, none of the PI3Kγ subunits were copurified with PDE3B-FLAG (data not shown). Therefore, it was concluded that $p87^{PIKAP}$ interacts with PDE3B. From cells cotransfected with PDE3B-FLAG, CFP-$p87^{PIKAP}$, and CFP-p110γ, both CFP-tagged proteins were coimmunoprecipitated upon IP with the anti-FLAG antibody (Fig. 4.23, *left panel*). However, CFP-$p87^{PIKAP}$ was copurified more efficiently than CFP-p110γ. Moreover, copurification of CFP-$p87^{PIKAP}$ was stronger if CFP-p110γ was absent. Both observations indicate that heterodimerization of $p87^{PIKAP}$ with p110γ may lower its affinity for PDE3B.

Consequently, it was investigated whether interaction of $p87^{PIKAP}$ with PDE3B modulates the activity of the latter. PDE assays were performed on lysates of HEK293 cells transfected with PDE3B-FLAG and different combinations of PI3Kγ subunits. In untransfected HEK293 cells, PDE3 activity was 8 ± 2 pmol/min/mg protein, assessed as the fraction of total PDE activity that was sensitive to the PDE3-specific inhibitor cilostamide. Expression of either p110γ or $p87^{PIKAP}$ did not alter the measured total and PDE3-specific activity (Fig. 4.24, *left panel*). Expression of PDE3B-FLAG led to a marked increase in PDE3 activity to 890 ± 210 pmol/min/mg protein. However, neither coexpression of p110γ or $p87^{PIKAP}$, nor of both p110γ and $p87^{PIKAP}$ significantly enhanced that activity (Fig. 4.24, *left panel*). A reduced PDE3 activity was observed upon coexpression of p101-FLAG. To exclude interference from variations in the expression level of PDE3B-FLAG, immunoblot experiments were performed. Surprisingly, coexpression of p101-FLAG led to decreased PDE3B-FLAG protein levels, whereas coexpression of $p87^{PIKAP}$ and p110γ did not affect expression of PDE3B-FLAG (Fig. 4.24, *blot in left panel*). It is thus likely that the reduction in PDE3 activity observed upon coexpression of p101-FLAG is chiefly due to a diminished expression of PDE3B-FLAG. Furthermore, it was tested whether exogenously applied purified $p87^{PIKAP}$ may yield a positive modulation of PDE3B activity. PDE3 activity was assayed in lysates of PDE3B-transfected HEK293 cells supplemented with 100 nM recombinant hexahistidine-tagged $p87^{PIKAP}$ that has been purified from baculovirus-infected Sf21 cells. Likewise, PDE3 activity remained unaltered (Fig. 4.24, *right panel*). Therefore, it may

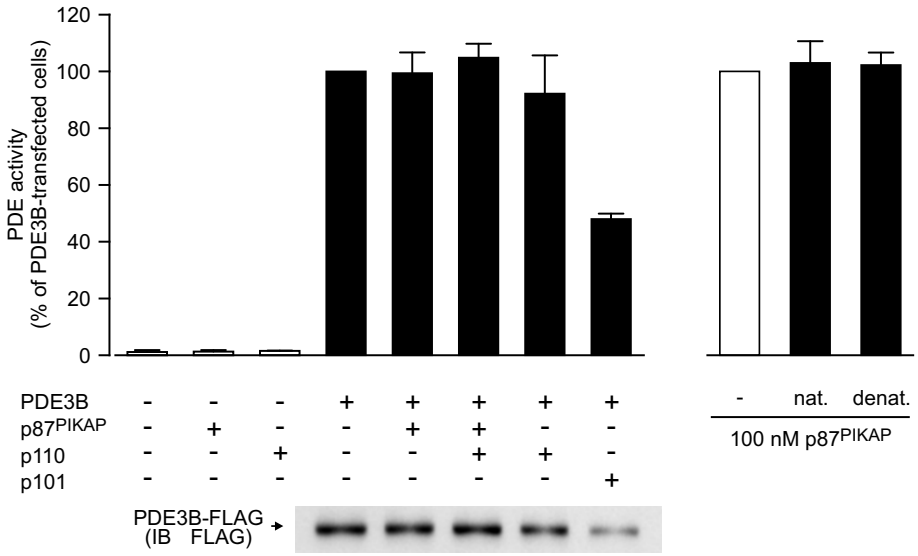

Figure 4.24: Effect of PI3Kγ subunit expression on PDE3B activity. *Left panel*, HEK293 cells were transfected with combinations of plasmids encoding the indicated FLAG-tagged proteins (the untagged version was used for p110γ). For PDE3B-FLAG, 0.2 μg of plasmid were used per transfection, while the amount of PI3Kγ subunit-encoding plasmid was 1.8 μg. PDE3 activity was assessed in cell lysates by determining PDE activity in the presence and absence of 10 μM cilostamide, a PDE3-specific PDE inhibitor. PDE3 activities were calculated as pmol/min/mg protein. To maintain comparability between different transfection experiments, activities were normalized to those obtained in lysates from HEK293 cells transfected with PDE3B-FLAG only. Means and S.E. of three independent transfection experiments are given. The expression of recombinant PDE3B-FLAG was analyzed by immunoblot with an anti-FLAG antibody, as shown below for a representative experiment. *Right panel*, lysates of HEK293 cells transfected with a plasmid encoding PDE3B-FLAG were incubated with 100 nM purified recombinant p87^{PIKAP} in native (nat.) or denatured (boiled for 5 min, denat.) state. Here, means and S.E. of two independent experiments are shown.

be inferred that p87^{PIKAP} both in monomeric form and in complex with p110γ is able to interact with PDE3B but that p87^{PIKAP} is not sufficient to modulate PDE3B activity.

4.2.7 Analysis of p87^{PIKAP} function by RNA interference

The phenomena of RNAi provide means to alter cellular processes by specifically and efficiently reducing the expression of a protein of interest. Thus, to analyze the function of p87^{PIKAP} in a more physiological setup, it was sought to establish a RNAi system for transient knockdown of p87^{PIKAP} and to apply it in a suitable model system. To expand the array of such potential model systems, the rat orthologue of p87^{PIKAP} was cloned from rat heart. Its sequence was determined and deposited in the DDBJ/EMBL/GenBank data bases under the accession number EF207569. The sequence is 94% identical on the nucleotide level and 96% identical on the protein level to that of the mouse orthologue in its slightly longer splice variant (accession number DQ295832).

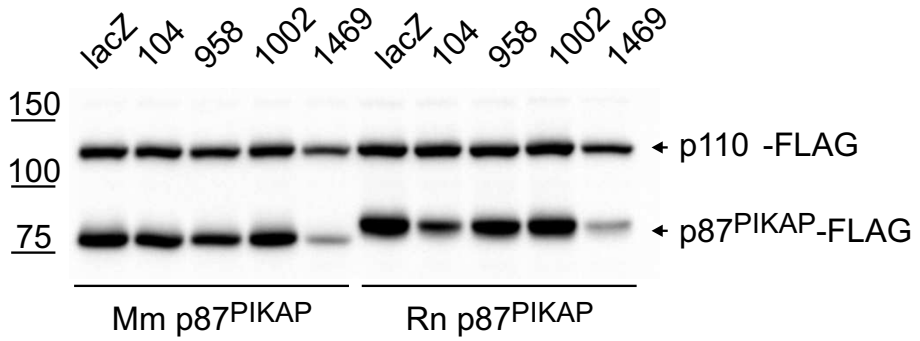

Figure 4.25: Knockdown of $p87^{PIKAP}$ expression by shRNA. HEK293 cells were transfected with p110γ-FLAG and either murine or rat $p87^{PIKAP}$-FLAG. Additionally, different shRNA plasmids based on the pENTR/H1/TO vector were cotransfected as indicated. Two days after transfection, whole cell lysates were prepared and analyzed by immunoblotting with an anti-FLAG antibody. The $p87^{PIKAP}$-specific shRNA plasmids are designated corresponding to their start position within the murine $p87^{PIKAP}$ coding sequence, while lacZ denotes a control construct that targets the lacZ-encoding sequence.

Four different target sequences identical in both the murine and rat $p87^{PIKAP}$ coding sequences were selected on the basis of prediction algorithms (see section 3.2.2 for sequences and details). To determine their actual effectiveness, the resulting shRNA plasmids were first assayed for their ability to interfere with the expression of $p87^{PIKAP}$ in transfected HEK293 cells. Of the four constructs tested, only one was able to significantly diminish the expression of both murine and rat $p87^{PIKAP}$ (Fig. 4.25). As expected, the lacZ shRNA control plasmid did not affect expression of $p87^{PIKAP}$. The pronounced knockdown observed for the pENTR-1469 shRNA vector suggests that it may induce silencing of sufficient extent in a native cellular system as well.

To identify a cell system that is characterized by selective expression of $p87^{PIKAP}$ with respect to p101 and that is amenable for genetic manipulation, further multiplex PCRs were performed. Results for a small selection of cell types tested are shown in Fig. 4.26. Although both p110γ and $p87^{PIKAP}$ messages were detectable in hearts of neonatal rats (Fig. 4.26), transfection of freshly prepared cardiac myocytes is known to be difficult. The HL-1 cell line, which was derived from

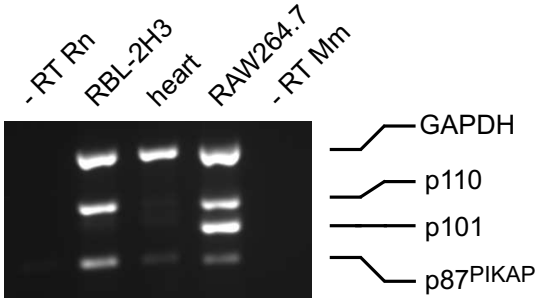

Figure 4.26: Expression of PI3Kγ subunits in a set of rat and murine cell types. Fragments of GAPDH, p110γ, p101, and $p87^{PIKAP}$ cDNA were simultaneously amplified by multiplex PCR on reverse-transcribed RNA from different sources. Because the primer sets partly differ for murine (Mm) and rat (Rn) orthologues, two reactions are shown that do not contain reverse-transcribed RNA. PCRs shown are representative of three experiments.

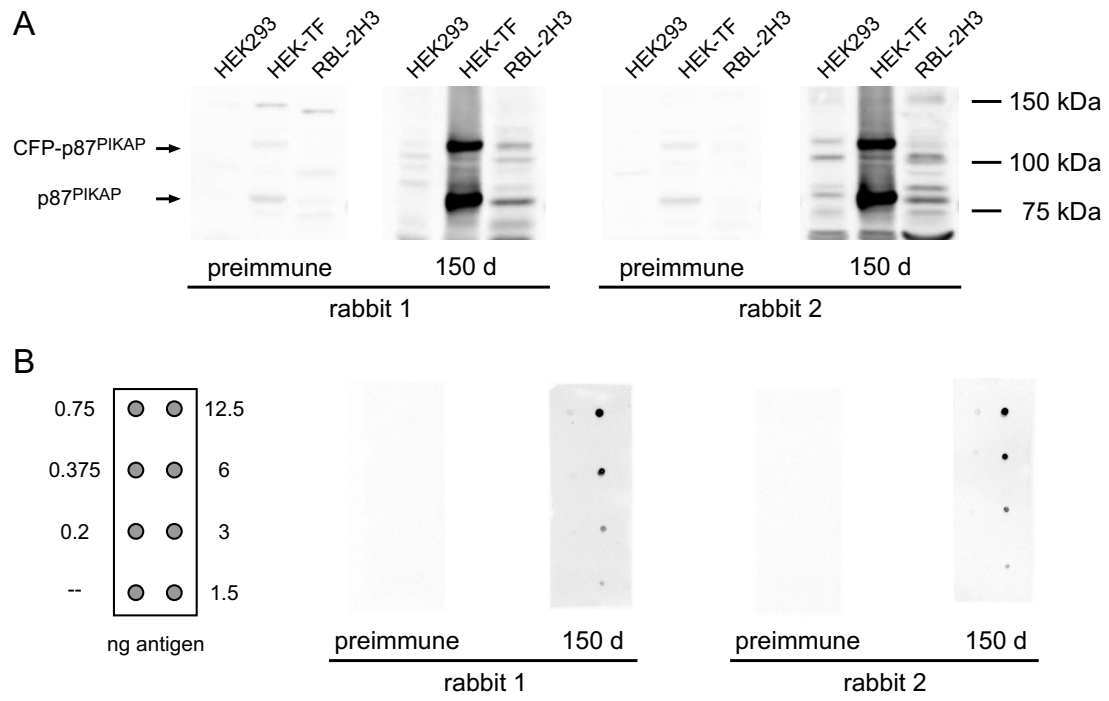

Figure 4.27: Generation of an antibody against p87^{PIKAP}. Two rabbits were immunized with purified recombinant His-tagged p87^{PIKAP} for 150 days, corresponding to eight immunization events. *A*, Western blot analysis employing preimmune sera and sera obtained after 150 days. Whole cell lysates of untransfected HEK293 cells expressing no p87^{PIKAP} (HEK293), HEK293 cells transfected with both wild-type and CFP-tagged p87^{PIKAP} (HEK-TF), and RBL-2H3 cells were separated by SDS-PAGE and assayed for p87^{PIKAP} expression with the indicated rabbit sera. *B*, Dot blot assay for the quantification of antibody sensitivity. A solution of the purified p87^{PIKAP} employed as the antigen was spotted on nitrocellulose membranes. The amount of protein applied is indicated in the scheme.

the murine AT-1 atrial tumor cell line, retains phenotypic characteristics of cardiac myocytes including noradrenaline-stimulated beating (Claycomb *et al.*, 1998). However, in contrast to organ-derived samples, p101 was more strongly expressed than p87^{PIKAP} in HL-1 cells, and expression of p110γ was severely reduced as well (data not shown). Therefore, additional leukocyte cell lines were assayed. In the macrophage cell line RAW264.7 the expression pattern was comparable to bone marrow-derived macrophages (see Fig. 4.22*A*), with p101 being expressed about twice as high as p87^{PIKAP} (Fig. 4.26). RBL-2H3 cells, however, showed prominent expression of p87^{PIKAP}, whereas p101 was absent (Fig. 4.26). RBL-2H3 cells share some features with mast cells, rendering them a well-established model for mast cell physiology. Moreover, it has been shown that degranulation of mast cells is amplified *via* a PI3Kγ-dependent autocrine feedback loop (see Introduction and Laffargue *et al.*, 2002). Thus, RBL-2H3 cells were chosen to investigate the effects of p87^{PIKAP} knockdown on a PI3Kγ-mediated signaling pathway.

First, the expression of p87^{PIKAP} in RBL-2H3 cells was verified on the protein level. To assess expression of p87^{PIKAP}, an antibody was employed that was raised against purified recombi-

nant His-tagged $p87^{PIKAP}$. A basal characterization of this antibody is shown in Fig. 4.27. A general increase in reactivity can be observed for post-immunization sera of both animals, and specific bands corresponding to $p87^{PIKAP}$ and CFP-$p87^{PIKAP}$ appeared in transfected HEK293 cells. These bands were not visible in the untransfected control cells. Using the serum of animal 1, a prominent band was discernible in lysates of RBL-2H3 cells that comigrated with the $p87^{PIKAP}$ band in the transfected HEK293 cells. Likewise, a band corresponding to $p87^{PIKAP}$ appears if serum of animal 2 was used. However, a number of unspecific bands with similar molecular weight hampered the use of unpurified sera derived from animal 2. Therefore, sera of animal 1 were used for further experiments. Both animals produced sera of comparable sensitivity towards the antigen, allowing detection of low ng amounts of $p87^{PIKAP}$ (Fig. 4.27*B*).

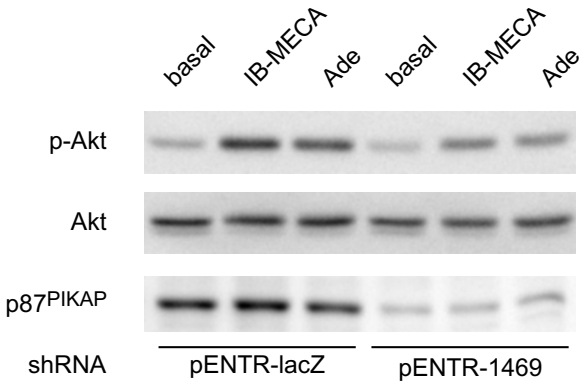

Figure 4.28: Akt phosphorylation in RBL-2H3 cells treated with $p87^{PIKAP}$ shRNA. RBL-2H3 were nucleofected with plasmids encoding a $p87^{PIKAP}$-directed shRNA (pENTR-1469) or a lacZ-directed control shRNA (pENTR-lacZ). Three days after nucleofection, cells were incubated with 200 ng/ml anti-DNP-BSA antibody for 3 h to obtain conditions comparable to the experiments in Fig. 4.29. Cells were then stimulated for 5 min with 10 μM IB-MECA or 10 μM adenosine. Western blots of whole cell lysates were probed with anti-phospho-Akt (Ser^{473}), anti-Akt, and anti-$p87^{PIKAP}$ antibodies. The results shown are representative of three independent nucleofection experiments.

Having confirmed the expression of $p87^{PIKAP}$ in RBL-2H3 cells, the impact of $p87^{PIKAP}$ knockdown on the phosphorylation of Akt upon stimulation of the G_i-coupled adenosine A_3 receptor was analyzed. The adenosine A_3 receptor has been shown to be the only adenosine receptor subtype involved in facilitation of mast cell degranulation both by expression studies and by investigating the sensitivity towards specific agonists and antagonists (Ramkumar *et al.*, 1993; Laffargue *et al.*, 2002). In RBL-2H3 cells transfected with the pENTR-1469 shRNA plasmid, expression of $p87^{PIKAP}$ was markedly reduced compared to cells transfected with the pENTR-lacZ control shRNA construct (Fig. 4.28), confirming the results obtained on transfected HEK293 cells. Stimulation with adenosine or the adenosine A_3 receptor-specific agonist IB-MECA led to a pronounced phosphorylation of Akt in lacZ-shRNA-expressing control cells, which was also evident from the slight gel shift of Akt (Fig. 4.28). In RBL-2H3 cells expressing $p87^{PIKAP}$-directed shRNA, however, phosphorylation of Akt was markedly reduced (Fig. 4.28),

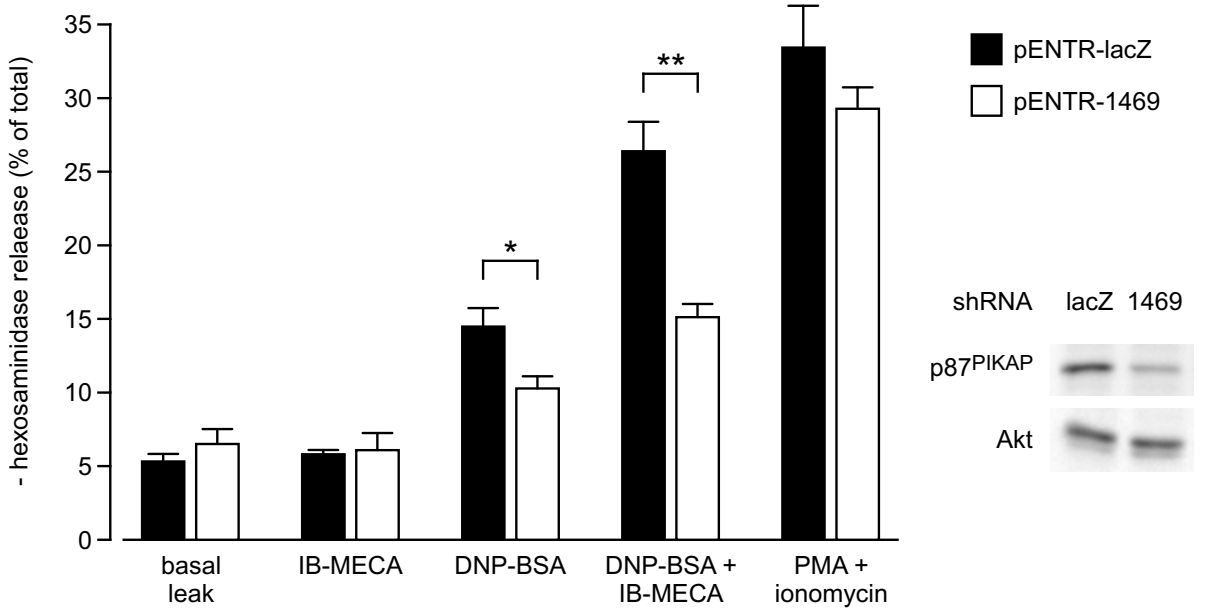

Figure 4.29: Knockdown of p87^{PIKAP} impedes adenosine receptor-mediated facilitation of degranulation in RBL-2H3 cells. RBL-2H3 were nucleofected with plasmids encoding a p87^{PIKAP}-directed shRNA (pENTR-1469; white bars) or a lacZ-directed control shRNA (pENTR-lacZ; black bars). Three days after nucleofection, cells were incubated with 200 ng/ml anti-DNP-BSA antibody for 3 h to sensitize cells for stimulation with the antigen DNP-BSA. Cells were incubated with different combinations of modulators for 30 min, before β-hexosaminidase activity released to the incubation buffer was determined. Release of β-hexosaminidase is given as the fraction of total cellular β-hexosaminidase content calculated from cell lysates and the basal leak. Concentrations of modulators were as follows: IB-MECA 10 μM, DNP-BSA 100 ng/ml, ionomycin 200 nM, PMA 50 nM. Presented are means and S.E. of three independent nucleofection experiments. A single asterisk indicates a difference significant at the $p < 0.05$ level, while two asterisks denote significance at the $p < 0.01$ level. Knockdown of p87^{PIKAP} was verified by Western blot analysis. A representative blot is shown.

indicating that expression of p87^{PIKAP} is crucial for PI3Kγ-mediated activation of Akt.

Next, it was analyzed whether knockdown of p87^{PIKAP} impairs the PI3Kγ-mediated amplification of degranulation in a similar way as the phosphorylation of the immediate downstream effector Akt. To this end, degranulation of RBL-2H3 cells expressing either lacZ-directed control shRNA or the p87^{PIKAP}-silencing 1469 shRNA was assessed as the amount of β-hexosaminidase – a commonly employed marker for exocytotic secretion in mast cells – released from the cells upon stimulation with antigen and IB-MECA. Stimulation with DNP-BSA, which induces clustering of the high-affinity FcϵRI receptors that were preoccupied with an anti-DNP antibody, led to release of about 15% of total β-hexosaminidase content of lacZ shRNA-treated RBL-2H3 cells (Fig. 4.29, *black bars*). Concomitant stimulation with IB-MECA enhanced degranulation considerably, as the amount of released β-hexosaminidase was almost doubled. In cells expressing the p87^{PIKAP}-silencing 1469 shRNA, the effect of IB-MECA was completely abolished (Fig. 4.29, *white bars*). Moreover, antigen-induced degranulation was significantly

reduced as well. In both cell populations, spontaneous degranulation was equal and remained unchanged in the presence of IB-MECA alone. Likewise, treatment with PMA and ionomycin, which leads to degranulation in a receptor-independent fashion (Katakami *et al.*, 1984; Cunha-Melo *et al.*, 1989), induced comparable release of β-hexosaminidase. These data indicate that p87^{PIKAP} may be indispensable for the action of PI3Kγ in the adenosine-mediated positive feedback loop that enhances the degranulation of mast cells.

4.3 Structural studies on the interaction of p101 and p87^{PIKAP} with p110γ and G$\beta\gamma$

In extension of the findings described in the first part of this thesis, it was sought to investigate the interaction of p101 and p87^{PIKAP} with p110γ and G$\beta\gamma$ in more detail. To this end, overlay experiments with peptide SPOT arrays were performed to identify peptide motifs within the primary structure of p101 and p87^{PIKAP} that are crucial for the interaction with p110γ and G$\beta\gamma$. Moreover, it was attempted to obtain pure heterodimeric p110γ/p87^{PIKAP} complexes and to initially characterize them with respect to their suitability for crystallization.

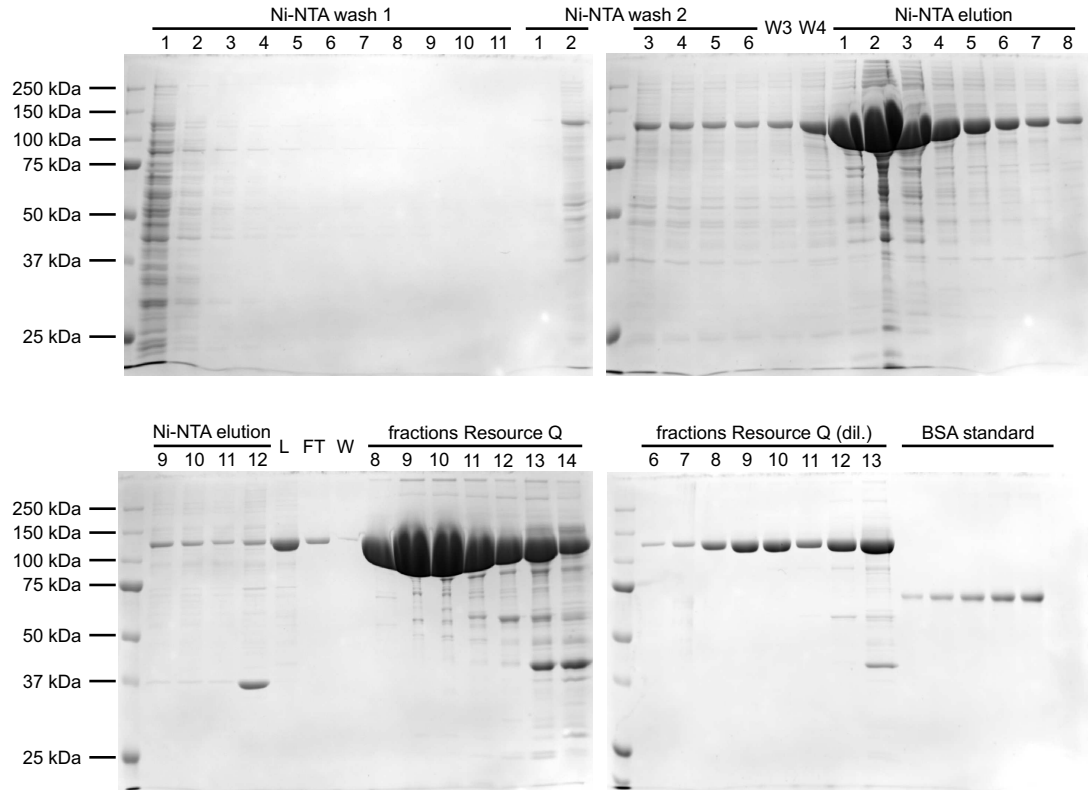

Figure 4.30: Purification of His-tagged p110γ from Sf21 cells. Sf21 cells were infected with a baculovirus encoding His-tagged p110γ and lysed 48 h after infection. Samples were taken at several steps of the purification process and analyzed by SDS-PAGE and Coomassie staining. Ni-NTA wash buffer contained either no imidazole (W1, W4), 10 mM imidazole (W2) or 20 mM imidazole (W3). The first 6 eluate fractions from the Ni-NTA column were pooled, diluted and applied to a Resource Q anion exchange column (load, L). Note that some protein was lost in the flow through (FT) and wash (W) due to weak affinity of the His-p110γ construct to the anion exchange resin. Protein was obtained by fractionated elution with a linear gradient of 0–1 M NaCl. The fractions containing the main peak were analyzed undiluted (lower left gel) to assess purity of His-p110γ. Additionally, 30–60-fold dilutions were processed together with BSA standards (0.2–1 μg) for an initial estimation of total yield (lower right gel).

4.3.1 Purification of proteins for peptide SPOT analysis

In order to probe peptide SPOT arrays, it is necessary to have the proteins to be bound in the overlay procedure available in reasonably pure form. Therefore, the purification of p110γ and G$\beta\gamma$ will be briefly described here. Both proteins were purified in recombinant form *via* Ni-NTA affinity chromatography. A representative purification of p110γ with a factor Xa-cleavable His tag is documented in Fig. 4.30. Typically, the yield was 10–14 mg of protein per liter Sf21 culture. The purification strategy using affinity chromatography and further purification and concentration on an anion exchange column proved feasible and yielded protein of high purity (see lower right gel in Fig. 4.30). Protein used to probe peptide SPOT membranes was taken from fractions 7–11. In a similar way, recombinant G$\beta\gamma$ complexes were purified

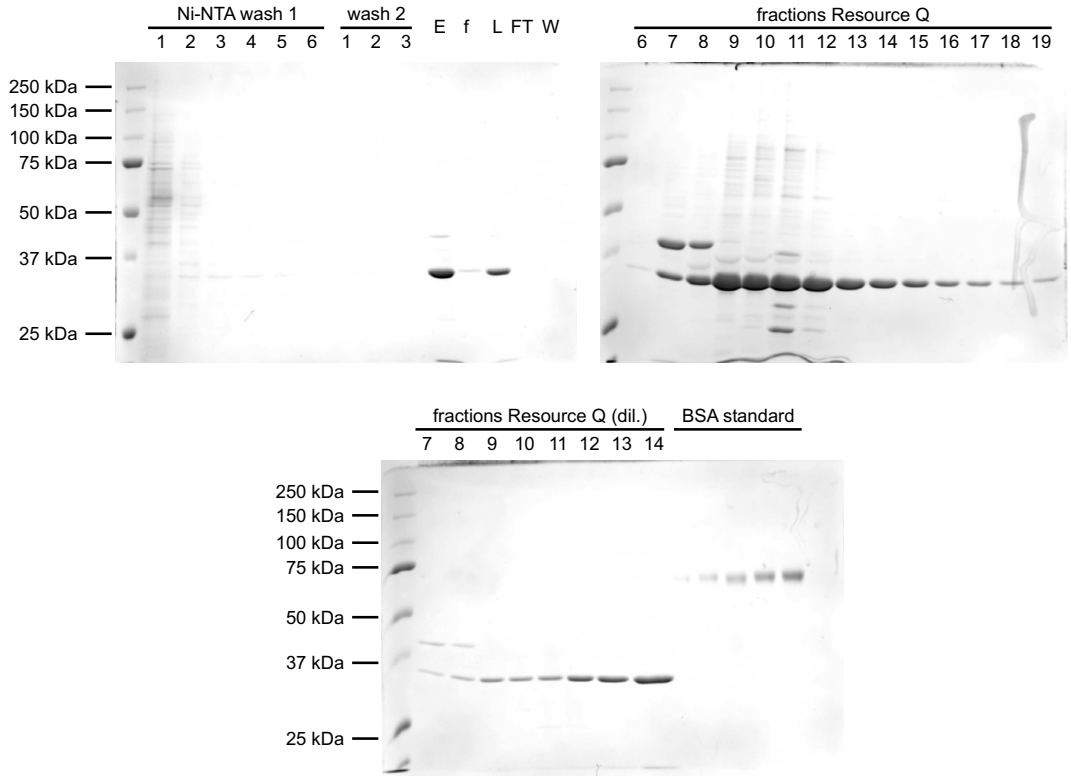

Figure 4.31: Purification of His-tagged G$\beta\gamma$ complexes from Sf21 cells. G$\beta\gamma$ complexes were purified from Sf21 cells infected with baculoviruses encoding Gβ_1 and His-tagged Gγ_2. The purification process was documented by SDS-PAGE and Coomassie staining. Ni-NTA wash 1 contained 20 mM imidazole, Ni-NTA wash 2 contained no imidazole and only 25 mM NaCl. The eluates from the Ni-NTA column were pooled (eluates, E), diluted twofold and applied to a Resource Q anion exchange column (load, L). After collecting the flow through (FT) and wash (W), fractionated elution was performed with a linear 0–1 M NaCl gradient. Fractions were analyzed either undiluted (upper right gel) to assess purity of recombinant G$\beta\gamma$ complexes. As above, 30–60-fold dilutions were used for an initial estimation of total yield by comparison with BSA standards (0.2–1 μg, lower gel).

and used for probing SPOT membranes to identify peptides on p101 and p87^{PIKAP} that interact with G$\beta\gamma$. The typical yield was 3–4 mg per liter Sf21 culture. Fractions 9–13 were used in subsequent overlay experiments.

4.3.2 Interaction of regulatory subunits with p110γ

At first, SPOT arrays of peptides were used that covered the whole sequence of p101 and p87^{PIKAP} piece by piece in peptides of 25 aa length, stepwise translated by 5 aa from N to C terminus, resulting in an overlap of 20 aa between adjacent peptides. This comparatively long peptide length was chosen because it allowed to cover the whole sequence of p101 and p87^{PIKAP} with a moderate number of peptides. Moreover, longer motifs important for the interaction may evade identification if too short peptides were used. A SPOT membrane with 25-aa peptides derived from full-length porcine p101 was subjected to an overlay procedure with purified p110γ. As expected from the characterization of p101 deletion mutants, signals were primarily detected for peptides corresponding to N-terminal regions of p101 (Fig. 4.32*A*, *left*). If the spot intensities were converted to the aa scale, 4 distinct regions within the N-terminal

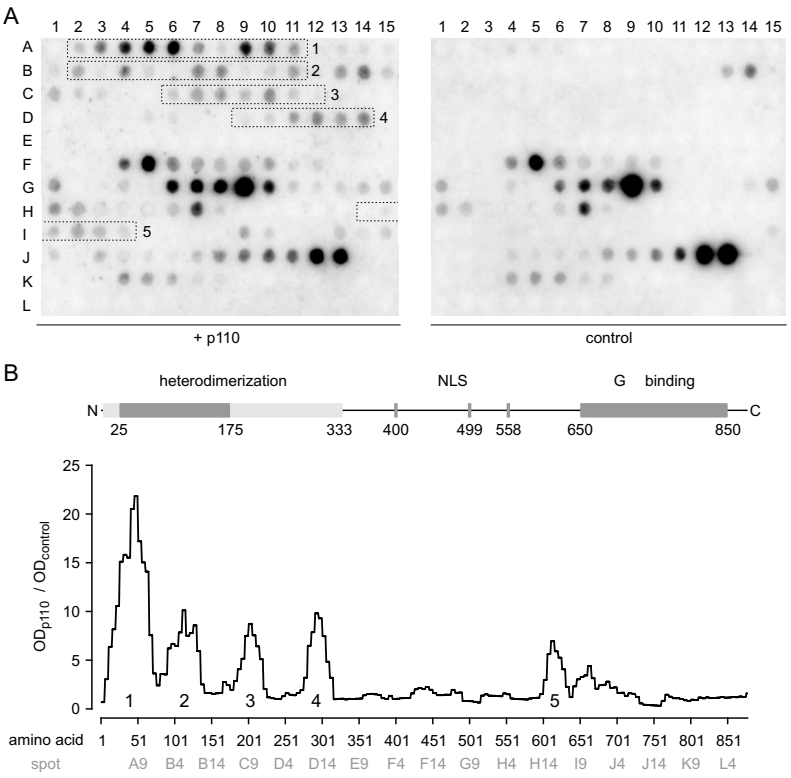

Figure 4.32: Peptide SPOT overlay of p101-derived peptides with p110γ. *A*, peptides of 25 aa length covering the sequence of p101 were SPOT-synthesized on cellulose membranes. One membrane was incubated overnight with His-tagged p110γ (+ p110γ), whereas the other remained in blocking buffer as a control for direct binding of the antibody to the spotted peptides (control). Bound His-tagged protein was detected with a HRP-coupled anti-His antibody. Clusters of positive signals were grouped and numbered. *B*, quantification of signal intensities and breakdown to single aa. Intensities were integrated for each spot, and intensity values for each aa were obtained by dividing spot intensities by 25 and summing over all peptides containing the aa. The domain structure of p101 is shown for orientation.

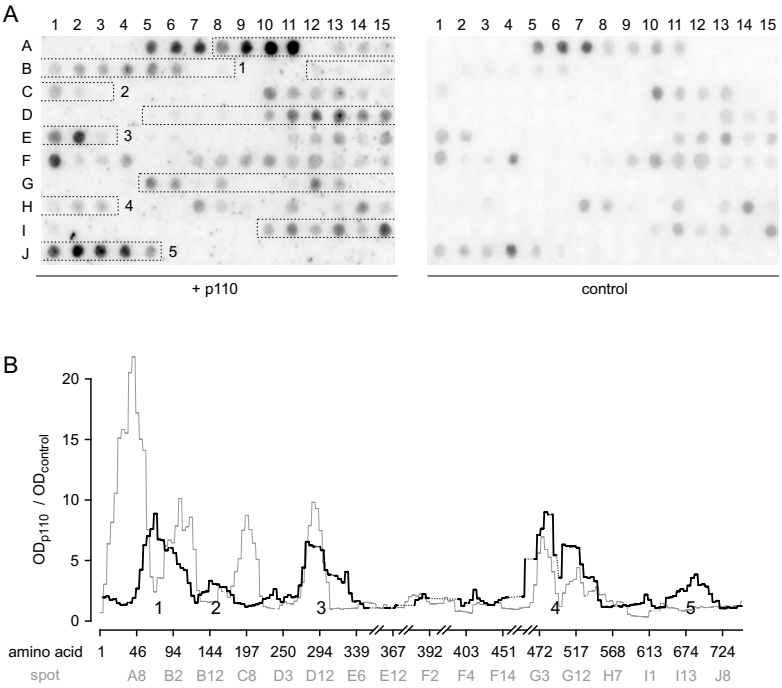

Figure 4.33: Overlay of p87^{PIKAP}-derived SPOT membranes with p110γ. *A*, peptides of 25 aa length covering the sequence of p87^{PIKAP} were synthesized on cellulose membranes. Control (control) and overlay membranes (+ p110γ) were treated and evaluated as described in Fig. 4.32. Positive signals were grouped and numbered. *B*, signal per aa was obtained as described in Fig. 4.32 and plotted over the p87^{PIKAP} sequence. Results for p101 are drawn in gray lines. Dashed parts indicate gaps arising from alignment of p101 and p87^{PIKAP} sequences.

~330 aa could be identified that correspond to clusters of positive spots (Fig. 4.32*B*). The antibody employed for detection of His-tagged p110γ exhibited high avidity towards many spots covering the middle part and C terminus of p101 (Fig. 4.32*A, right*). These spots did not show significant differences between p110γ-incubated and control membranes, indicating the absence of p110γ binding. However, for a cluster of spots within the C terminus, weak binding of p110γ could be observed (Fig. 4.32*A, left, box 5*).

The experiment was repeated using membranes containing peptides based on the murine p87^{PIKAP} sequence. Although many spots already showed weak to moderate staining upon incubation with the antibody (Fig. 4.33*A, right*), a range of peptides could be identified that displayed significantly enhanced signals upon overlay with His-tagged p110γ. As observed for p101, the most intense spots that were recognized by p110γ were located within the N terminus of p87^{PIKAP} (Fig. 4.33*A, left*). The first cluster overlaps with the first two regions recognized in p101, whereas the second precedes the third one of p101 (Fig. 4.33*B*). Around aa 300, responses were comparable for both p101 and p87^{PIKAP}. Within the C terminus, a region corresponding to that identified in p101 showed positive spots as well (block 4), but another set of spots exhibited affinity for p110γ that contained peptide sequences corresponding to the far C terminus (block 5, Fig. 4.33*A,B*). Thus, these findings support the similarity-based assumption that the N terminus may function as the heterodimerization domain in p87^{PIKAP} like it does in p101. However, an epitope that exhibits affinity for p110γ may also be found in a region located N-terminal of the G$\beta\gamma$ binding domain.

In an attempt to both validate these findings and to enhance the resolution of the binding

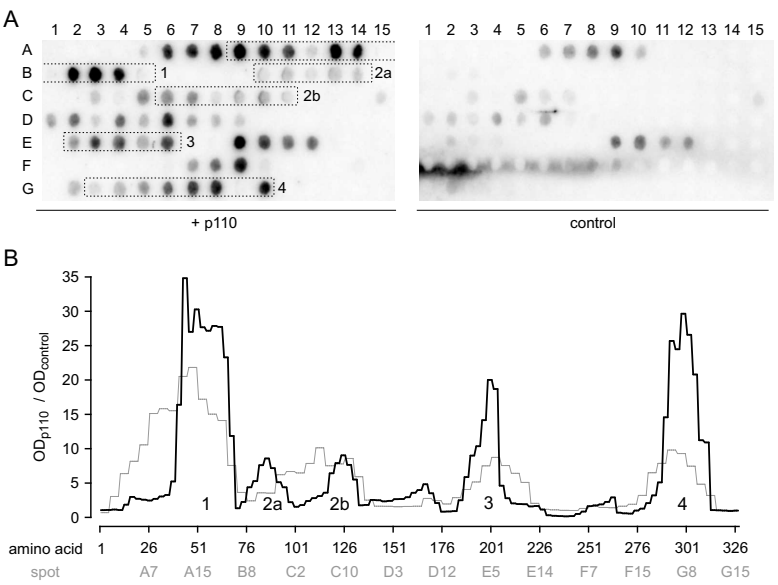

Figure 4.34: Binding of p110γ to the N terminus of p101. *A,B*, SPOT-synthesized peptides of 15 aa length covering the N terminus of p101 were assayed for binding of His-tagged p110γ (+ p110γ; untreated control, control) and evaluated as described in Fig. 4.32. Positive signals were grouped and numbered corresponding to the scheme introduced in Fig. 4.32. In *B*, signal intensities were plotted per aa in black for the present membrane and in gray for the 25-aa peptide membrane depicted in Fig. 4.32.

screen, membranes were used containing peptides of 15 aa length, translated along the sequence by 3 aa each, giving rise to peptides with 12-aa overlap. Although longer motifs may be lost by shortening the SPOT-synthesized peptides, shorter peptides allow finer mapping and have the advantage of leading to higher yield of full-length peptide in synthesis. Moreover, known linear peptide epitopes involved in the interaction of signaling proteins are often relatively short (see examples *e.g.* in Neduva & Russell, 2006). To reduce the number of spots, the sequences displayed on these membranes were confined to 330 aa each at the N and C terminus of p101 and p87$^{\text{PIKAP}}$.

The results for the N terminus of p101 are shown in Fig. 4.34. If the intensities were compared in an aa-based form, the pattern of p110γ-binding aa largely resembled that obtained for 25-aa peptides (Fig. 4.34*B*). Use of 15-aa peptides, however, resulted in sharper peaks and higher resolution on the aa level. The first cluster of positive spots appeared more narrow compared to the 25-aa peptide screen. This may either indicate that, of the positive spots obtained for the far N terminus (A2–A5, Fig. 4.32*A*), mainly the C termini contributed to capture of p110γ, or that an eventual binding of p110γ to spots A6–A8 is masked by the unspecific binding of the antibody (compare Fig. 4.34*A*, *left* and *right*). The second region identified above was found split in two areas, while both the third and fourth one were confirmed largely within the same borders as above (see Fig. 4.32). Still, by producing steeper increases in signal intensities, the data derived from the 15-aa peptide screen may allow a narrower allocation of the aa that mainly contribute to binding.

The fifth group of labeled spots, which corresponded to a C-terminal sequence in p101 (see Fig. 4.32), was also confirmed using shorter peptides (Fig. 4.35*A*, spots A2-A6). In addition, two smaller sets of spots were also labeled in a p110γ-specific fashion (Fig. 4.35*A*, spots B2–B4 and

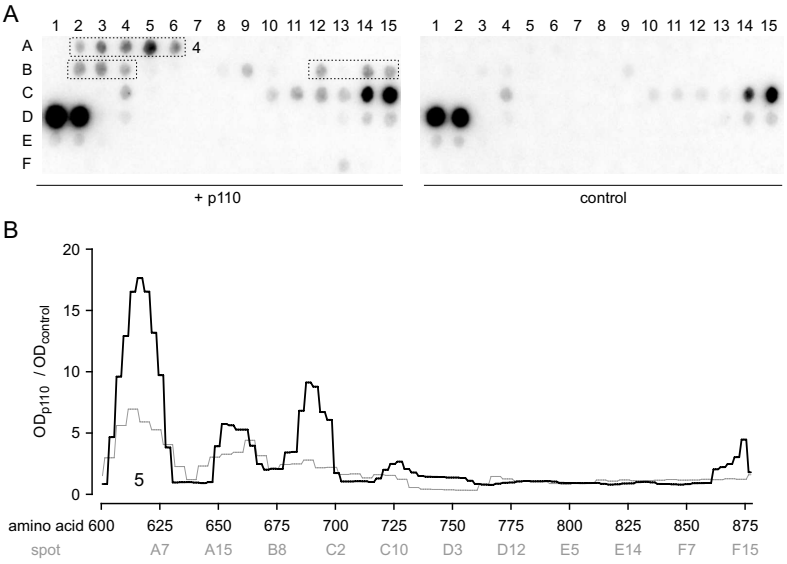

Figure 4.35: Binding of p110γ to the C terminus of p101. *A,B*, SPOT-synthesized peptides of 15 aa length covering the C terminus of p101 were analyzed for binding of His-tagged p110γ and evaluated as described in Fig. 4.32. Positive signals were grouped and numbered corresponding to the scheme introduced in Fig. 4.32. In *B*, signal intensities were plotted over the C-terminal sequence of p101 (black, 15-aa membrane from part *A*, gray, 25-aa membrane from Fig. 4.32).

B12–B15), which were not obvious from the previous membrane containing 25-aa peptides.

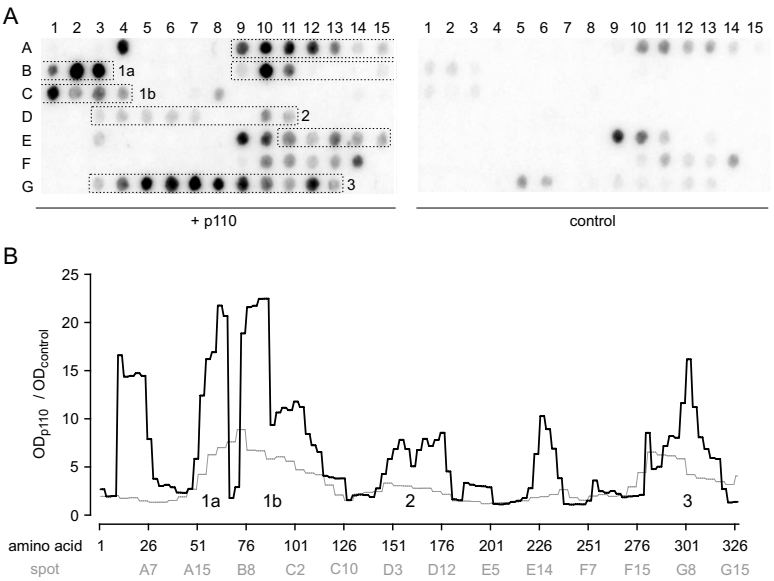

Figure 4.36: Binding of p110γ to the N terminus of p87^{PIKAP}. *A,B*, SPOT-synthesized peptides of 15 aa length covering the N terminal 327 aa of p87^{PIKAP} were assayed for binding of His-tagged p110γ (+ p110γ; untreated control, control) and evaluated as described in Fig. 4.32. Positive signals were grouped and numbered corresponding to the scheme introduced in Fig. 4.33. In *B*, signal intensities were plotted per aa in black for the present membrane and in gray for the 25-aa peptide membrane depicted in Fig. 4.33.

Analogous membranes based on the p87^{PIKAP} sequence were also probed. Within the N terminus, the first set of peptides that correspond to those exhibiting binding to p110γ as 25-aa peptides (see Fig. 4.33) was found split in two distinct groups of peptides (1a,1b in Fig. 4.36*A,B*). The blocks labeled with 2 and 3 match those found in Fig. 4.33, whereas p110γ exhibited affinity towards a number of spots that were located in between, around aa 226 (Fig. 4.36*A*). A single spot of high intensity at the far N terminus (A4) was also observed. For the C terminus of p87^{PIKAP}, essentially the same aa appeared to be recognized by His-tagged p110γ as in Fig.

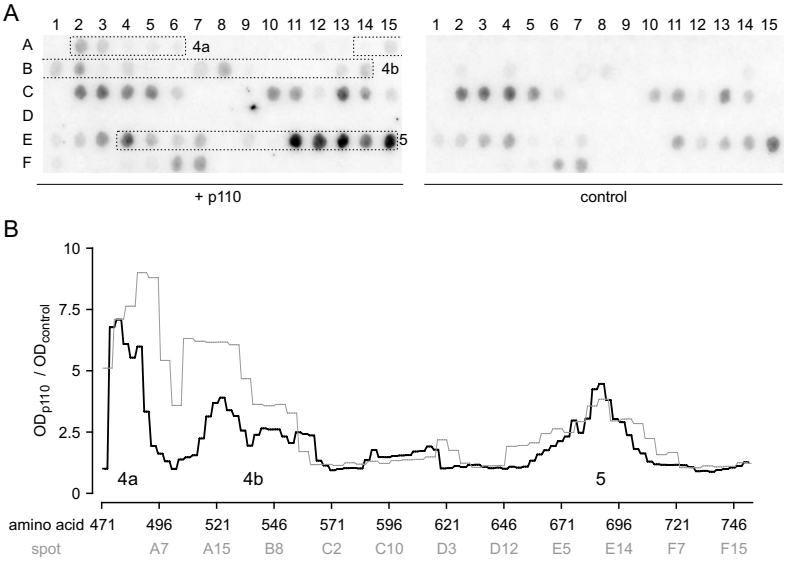

Figure 4.37: p110γ overlay on spots covering the C terminus of p87^{PIKAP}. *A,B*, SPOT-synthesized peptides covering aa 471–752 of p87^{PIKAP} were probed for binding of His-tagged p110γ as described in Fig. 4.32. Numbering of peptide clusters is as in Fig. 4.33. In *B*, signal intensities were plotted per aa in black for the membrane shown in *A* and in gray for the 25-aa peptide membrane shown in Fig. 4.33.

4.33. Generally, the signal intensities were much weaker than for the N-terminal peptides detected (compare Fig. 4.36). Those corresponding to the fourth region were found split in two subgroups (4a,4b in Fig. 4.37).

Taken together, several regions within p101 and p87^{PIKAP} were identified that are recognized by p110γ. In the subsequent deduction of peptide sequences that may be crucial for interaction between p110γ and its regulatory subunits, it was focused on elements present in both p101 and p87^{PIKAP}. For those areas of p101 and p87^{PIKAP} that exhibited similar clusters of spots, the aa-based intensities were examined together with a set of sequences of p101 and p87^{PIKAP} orthologues. Thereby, the conservation of certain residues may provide additional hints towards aa crucially involved in the interaction.

Within the N terminus, 4 clusters were selected (Fig. 4.38). Although the tripeptide 'WSL' is conserved throughout p101 and p87^{PIKAP} orthologues (Fig. 4.38*A*), it appears mainly to contribute to binding in p101 but not p87^{PIKAP}. However, strong binding of the antibody alone to this epitope on p87^{PIKAP}-derived SPOT membranes (see spots A10–A13 in Fig. 4.36*A*) may have masked binding of p110γ. This tripeptide is followed by a set of largely conserved residues including both hydrophobic and charged side chains such as Val 48, Arg 50, Asp 51, Pro 53, and Gly 54. Starting with the rigorously conserved Leu 58, a stretch containing a high number of charged residues is found, which were recognized by p110γ in both p101 and p87^{PIKAP}-derived peptides. Besides adding up to similar net charge, these residues, however, do not exhibit any features conserved between p101 and p87^{PIKAP}. A characteristic of region 2a of p101 and 1b of p87^{PIKAP}, respectively, is a conserved PL dipeptide in a largely apolar environment containing also a Tyr, which is central to the stretch exhibiting affinity towards p110γ in both p101 and p87^{PIKAP} (Tyr 86 in p101, Tyr 82 in p87^{PIKAP}, Fig. 4.38*B*). At the intersection of regions 2b of p101 and 1b of p87^{PIKAP}, a number of fully conserved residues followed by a still highly conserved

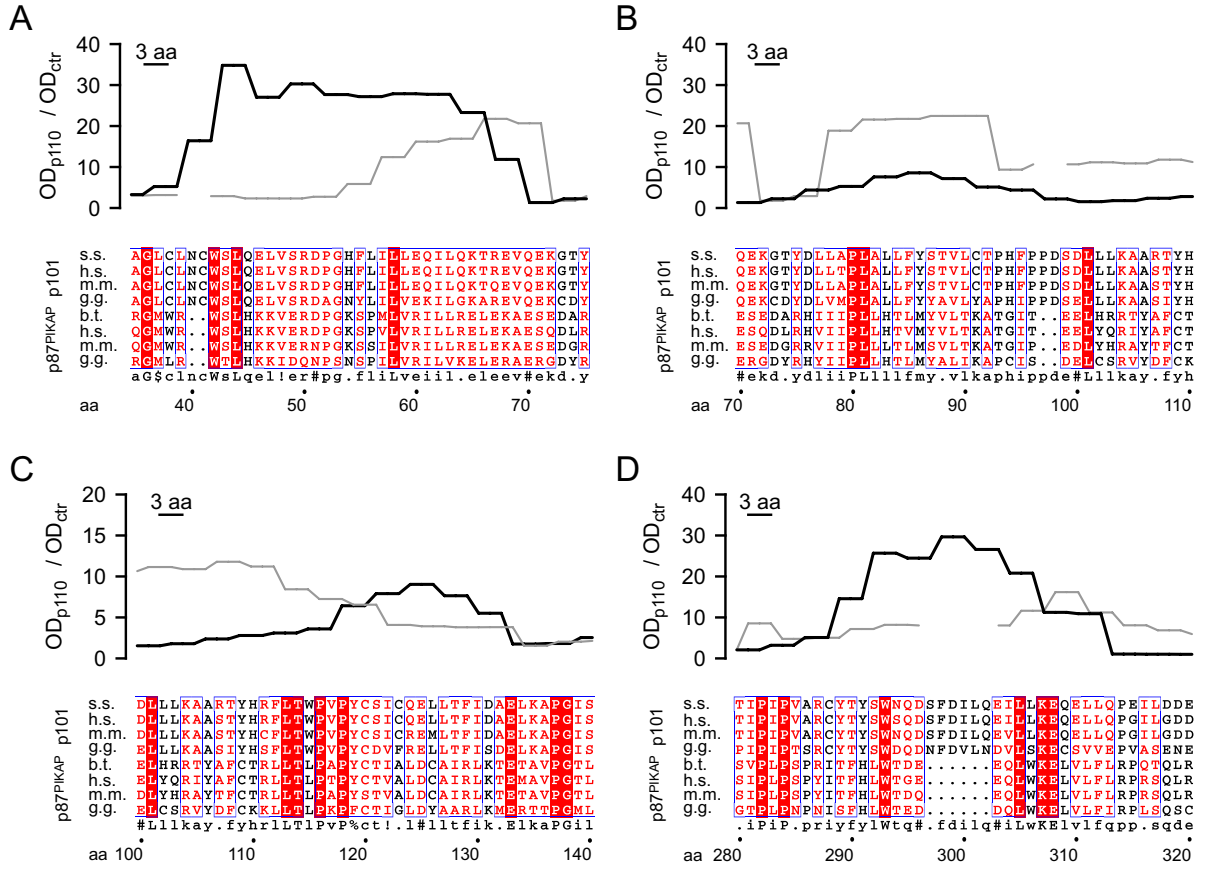

Figure 4.38: N-terminal peptide sequences involved in binding to p110γ in p101 and p87^{PIKAP}. The aa-based signal intensities computed in Fig. 4.34 for p101 and in Fig. 4.36 for p87^{PIKAP} were plotted over an alignment of a set of p101 and p87^{PIKAP} orthologues (p101, black, p87^{PIKAP}, gray lines). Depicted are sequence areas corresponding to cluster 1 of p101/ 1a of p87^{PIKAP} (*A*), 2a of p101/1b of p87^{PIKAP} (*B*), 2b of p101/ 1b of p87^{PIKAP} (*C*), and 4 of p101/ 3 of p87^{PIKAP} (*D*, compare also Fig. 4.34 and 4.36). The align was generated using ClustalW and ESPript. Numbering is based on porcine p101. A consensus sequence is given, where uppercase and lowercase letters indicate complete and >50% conservation, respectively. ! represents I or V, $ L or M, % F or Y, and # N, D, Q, or E. Abbreviations of species names: s.s., *sus scrofa* (pig); h.s., *homo sapiens* (human); m.m., *mus musculus* (mouse); g.g., *gallus gallus* (chicken); b.t., *bos tauris* (cow). The latter was taken for p87^{PIKAP}, because a porcine p87^{PIKAP} sequence has not been reported yet.

Tyr residue stand out (Fig. 4.38*C*). In the following stretch, two conserved acidic positions are found (Fig. 4.38*C*, Glu 125 and Glu 133 of porcine p101). The N-terminal third ends with a region exhibiting high affinity to p110γ in both p101 and p87^{PIKAP} (Fig. 4.38*D*). It commences with two conserved Pro residues that may be employed in a reorientation of the polypeptide chain towards a complementary binding site on p110γ. The following set of aa centered around a conserved Trp features many residues containing functional groups such as Arg, Tyr, Thr, Ser, and acidic residues (Fig. 4.38*D*, residues 287–296 of porcine p101). Peculiarly, a stretch of six aa separates these residues from the next set of conserved residues in p101 but not in p87^{PIKAP}.

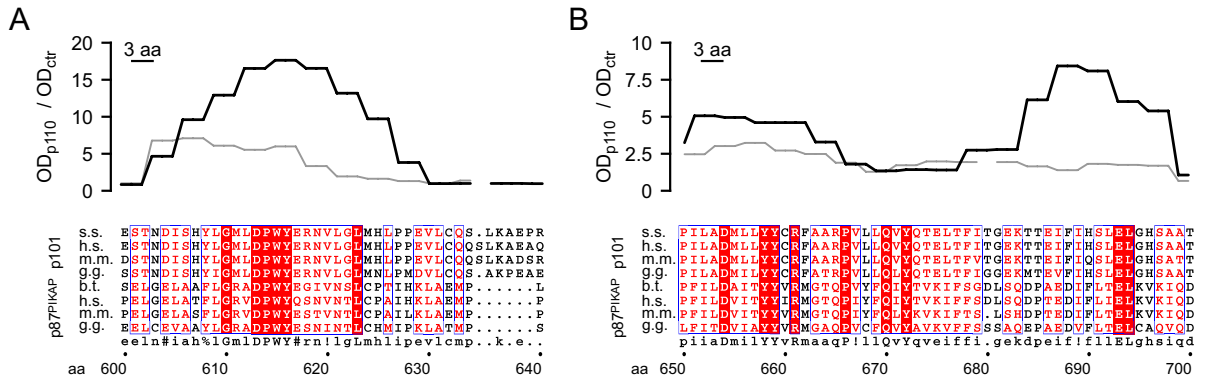

Figure 4.39: C-terminal p110γ-binding peptide sequences identified by peptide SPOT overlay assays. Signal intensities computed in Fig. 4.35 (p101) and Fig. 4.37 (p87^{PIKAP}) are given along with an alignment of a set of p101 and p87^{PIKAP} orthologues. Depicted are sequence areas corresponding to cluster 5 of p101/ 4a of p87^{PIKAP} (*A*), and 4b of p87^{PIKAP} (*B*, compare Fig. 4.35 and 4.37). Abbreviations are the same as in Fig. 4.38.

These conserved residues begin with an acidic aa followed by largely hydrophobic side chains and a KE dipeptide, indicating a possible shielded electrostatic interaction (Fig. 4.38*D*).

Within the C terminus, mainly two epitopes stand out. The first well-conserved stretch begins with a conserved acidic residue (Asp 604 of porcine p101) that is followed by an aromatic function (Tyr 608) before a conserved Gly and a distinctive 'DPWY' peptide closed of by a largely conserved Glu (Fig. 4.39*A*). The second epitope starts with hydrophobic residues embedding a conserved Asp, and that area is continued by a YY dipeptide and a single Arg, both completely conserved between p101 and p87^{PIKAP} in different species (Fig. 4.39*B*). About 30 aa towards the C terminus, another stretch is present where peptides recognized by p110γ were detected. It, however, contains only a Glu conserved in p101 and p87^{PIKAP} in adjacent positions and an EL dipeptide as striking features (Fig. 4.39*B*, aa 686–696 of p101).

4.3.3 Interaction of regulatory subunits with G$\beta\gamma$

In addition to dimerization with p110γ, interaction with G$\beta\gamma$ is a hallmark of p101 and p87^{PIKAP} function. To resolve which motifs within the regulatory subunits are employed in interaction with G$\beta\gamma$, peptide SPOT overlay assays were performed in a similar fashion as described above for p110γ binding. Although the G$\beta\gamma$ binding domain was mapped to the C-terminal aa 650–850 of p101, analysis commenced with the same 25-aa peptide membranes spanning the whole sequence of p101 and p87^{PIKAP} as used before. In doing so, minor elements outside the mapped region that contribute to G$\beta\gamma$ binding may be identified. All membranes assayed contained two peptides known to bind G$\beta\gamma$ with high affinity (the so-called SIGK peptide and an optimized analogue; both described in Scott *et al.*, 2001) as positive controls.

These positive controls showed strong signals on the p101 and p87^{PIKAP} membranes with 25-aa peptides (Fig. 4.40*A*, spots L13 and L14 for p101, spots J13 and J14 for p87^{PIKAP}). How-

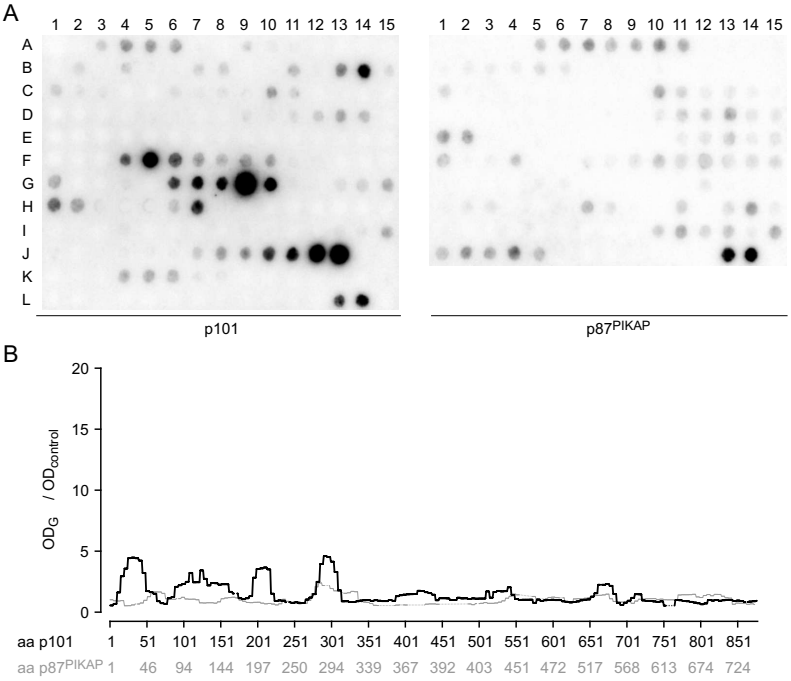

Figure 4.40: G$\beta\gamma$ overlay assays on p101 and p87^{PIKAP} SPOT membranes. *A*, membranes identical to those probed with His-tagged p110γ in Fig. 4.32 (p101, left) and 4.33 (p87^{PIKAP}, right) were subjected to overlay assays with G$\beta_1\gamma_{2-His}$ as the probe. For negative controls without protein see Fig. 4.32*A* (p101) and 4.33*A* (p87^{PIKAP}). *B*, spot signal intensities were converted to the aa level and plotted over the aligned sequences of p101 (black) and p87^{PIKAP} (gray). Dotted lines indicate sequence gaps.

ever, the remaining spot pattern corresponded largely to that of the membranes incubated with the detection antibody only (see membranes indicated with *control* in Fig. 4.32*A* and 4.33*A*). Thus, for neither p101 nor p87^{PIKAP} peptides could be retrieved that exhibit significant affinity towards G$\beta\gamma$. The efficiency and yield of peptide synthesis in general and especially if performed in a membrane-coupled fashion is strongly dependent on peptide length. Therefore, the absence of positive signals from p101- or p87^{PIKAP}-derived peptides may have resulted from inefficient synthesis of the comparatively long peptides. Indeed, subsequent Ponceau staining of the membranes revealed that several spots within the C-terminal region, for which binding peptides were expected, exhibit low amounts of detectable peptide (data not shown). To reduce interference from synthesis artifacts, the 15-aa peptide membranes corresponding to the C termini of p101 and p87^{PIKAP}, which are likely involved in interaction with G$\beta\gamma$, were assayed in the same way.

Again, the positive controls yielded very intense signals (Fig. 4.41*A*, spots G1 and G2 for each p101 and p87^{PIKAP}). For p101, essentially the same spots as those labeled by p110γ were also bound by G$\beta\gamma$, although with about 2-fold lesser intensity (Fig. 4.41*A, left* and *B*, compare Fig. 4.39). For p87^{PIKAP}, significant changes compared to the negative control (depicted in Fig. 4.35*A* for p101 and 4.37*A* for p87^{PIKAP}) were not detectable (Fig. 4.41*A, right*). Ponceau staining of these membranes also revealed that a number of spots on both membranes show little density of Ponceau-stainable peptide (data not shown).

In a reciprocal approach, SPOT arrays of peptides covering the sequence of Gβ_1 were analyzed for affinity towards PI3Kγ. Since Gγ does not provide major interaction sites in most G$\beta\gamma$-effector interactions, it was omitted from the analysis. Attempts failed to purify the G$\beta\gamma$

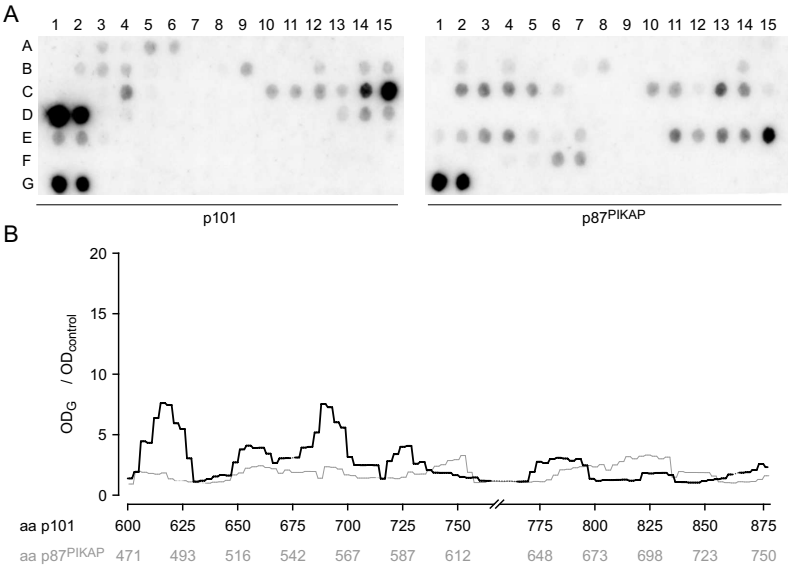

Figure 4.41: G$\beta\gamma$ overlay assays with peptide arrays covering the C terminus of p101 and p87$^{\mathbf{PIKAP}}$. *A*, overlay assays with $G\beta_1\gamma_{2-His}$ on membranes as those probed with His-tagged p110γ in Fig. 4.35 (p101, left) and 4.37 (p87^{PIKAP}, right). For negative controls without protein incubation see Fig. 4.35*A* (p101) and 4.37*A* (p87^{PIKAP}). *B*, spot signal intensities were converted to the aa level and given over the aligned sequences of p101 (black) and p87^{PIKAP} (gray). Dotted lines indicate sequence gaps.

binding domain of p101 in sufficient quantity for overlay assays (data not shown). Therefore, it was resorted to heterodimeric PI3Kγ complexes. Purification of the His-p110γ/p87^{PIKAP} dimers employed in these assays is shown below in Fig. 4.44. In contrast to the other membranes probed previously, groups of positive peptides contained mostly 2–3 peptides only (Fig. 4.42*A*, left). Thus, comparatively narrow sequence stretches were obtained when peptide signals were broken down to contributions from single aa (Fig. 4.42*B*). As three-dimensional structures are available for G$\beta\gamma$ complexes, the positions of the identified aa could be allocated to structural correlates (Fig. 4.42*C*). Among a plethora of studies concerning the interaction between G$\beta\gamma$ and its effectors, data from co-crystals containing peptides identified in phage-display experiments (Scott *et al.*, 2001; Davis *et al.*, 2005) were used for an initial assessment of the data obtained here. Several of the aa on top of the β propeller that are involved in binding of the SIGK peptide were also recognized by the PI3Kγ heterodimer, including Gln 75, Trp 99, Met 101, Tyr 145, Asp 246, and Trp 332 (Fig. 4.42*C*, red residues). Moreover, an additional loop was found to contribute to binding that is covered by spot cluster 5. It contains both aromatic (Tyr 289, Phe 292) and acidic (Asp 290 and 291) residues. In general, mostly peptides were labeled by the His-p110γ/p87^{PIKAP} dimers that cover loops on top of the β propeller and their extensions but only few that correspond to surfaces on the side of the propeller.

4.3.4 Purification of heterodimeric PI3Kγ for crystallization

The most complete knowledge concerning the structural aspects of the interaction between p110γ and its regulatory subunits can be derived from crystallographic analysis of the heterodimeric protein complexes. Therefore, it was attempted to obtain p110γ/p87^{PIKAP} complexes of high purity and sufficient quantity for initial crystallization screens. p87^{PIKAP} was

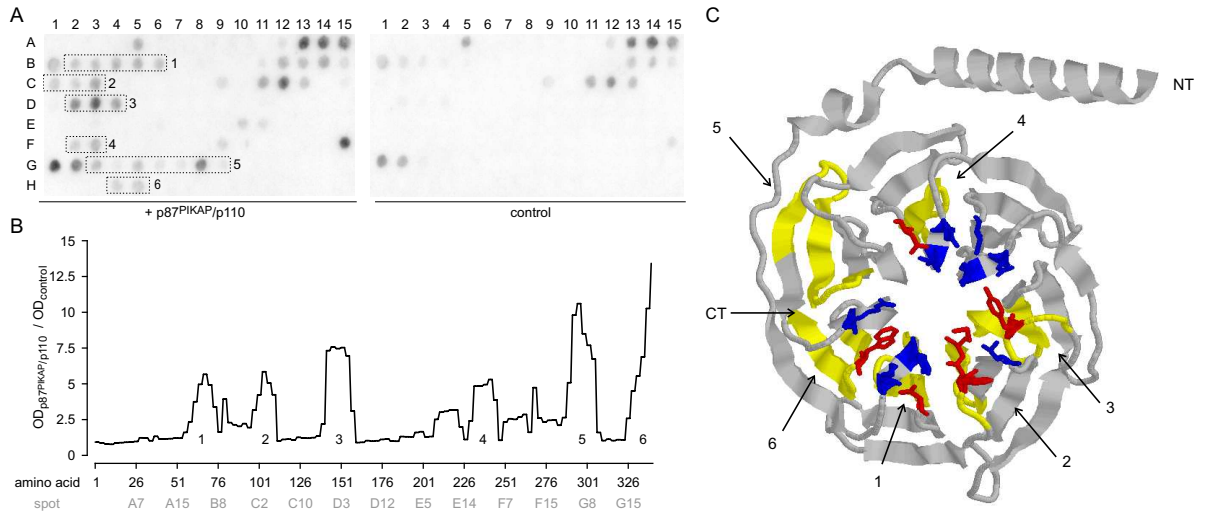

Figure 4.42: Overlay assay of Gβ_1-derived peptides with heterodimeric PI3Kγ. *A*, membranes containing 15-aa peptides derived from the sequence of Gβ_1 were probed with His-tagged p110γ/p87^{PIKAP} complexes or left untreated. *B*, spot signal intensities were converted to the aa level and plotted against aa number. Spot positions are given in gray. *C*, position of PI3Kγ-binding peptides within the three-dimensional structure of Gβ_1. Sequences, for which the aa-based signal exceeds 3, are given in yellow and are numbered as in *B*. Residues closer than 5 Å to any atom of the G$\beta\gamma$-binding SIGK peptide are represented by blue stick models. Those residues that contact both SIGK peptide and PI3Kγ are colored red. Coordinates were taken from the G$\beta\gamma$-SIGK peptide complex (1XHM PBD data set). The figure was generated with Rasmol.

chosen instead of p101, because purification of p101 both in monomeric form and in complex with p110γ had been performed previously by several groups (see *e.g.* Stephens *et al.*, 1997; Maier *et al.*, 1999) and is known to result in poor yield. The smaller size and higher stability of p87^{PIKAP} may be beneficial in purification of PI3Kγ complexes. Moreover, its novelty and the fact that it was identified in the course of this thesis added to the decision in favor of p87^{PIKAP}.

At first, p110γ and p87^{PIKAP} were coexpressed both as His-tagged proteins in Sf21 cells. Because the strategy had been successfully used for the purification of His-tagged p110γ, Ni-NTA affinity chromatography was combined with anion exchange chromatography. A representative preparation is shown in Fig. 4.43. Both subunits were present in the eluates from the metal affinity column. Presumably due to the presence of two His tags in the complex, the p110γ/p87^{PIKAP} dimer eluted in a rather broad peak so that the first 7 fractions were combined for further processing. Binding of the complex to the column material was comparatively weak, because it eluted already with salt concentrations of ~120 mM NaCl. Except for a prominent band at ~40 kDa appearing in fractions 13–15, peak fractions containing heterodimeric PI3Kγ exhibited higher concentration and purity as the eluates obtained from the Ni-NTA column. Given that monomeric His-tagged p110γ eluted from the anion exchange column in early fractions as well (see Fig. 4.30), analytical gel filtration was performed to verify the presence of heterodimeric complexes and to exclude contaminations from an excess of either His-tagged

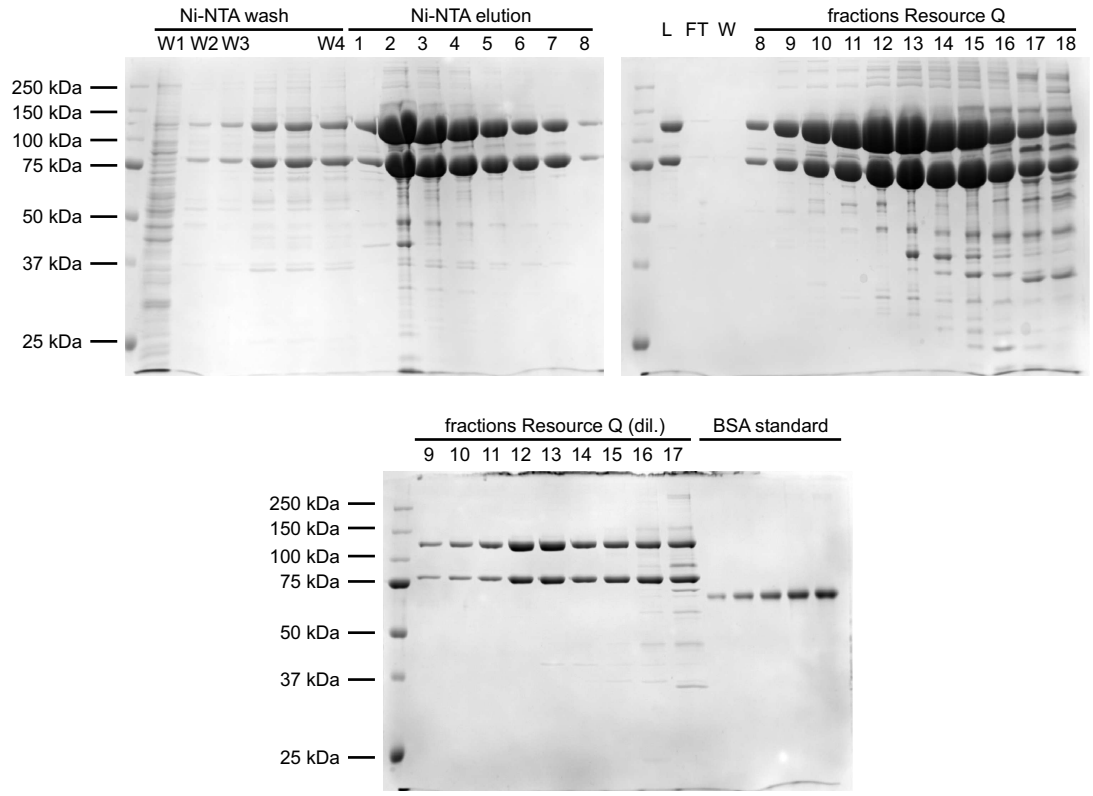

Figure 4.43: Purification of heterodimeric p110γ/p87^{PIKAP} complexes from Sf21 cells. Sf21 cells were infected with baculoviruses encoding His-tagged p110γ and His-tagged p87^{PIKAP}, and cell lysates were prepared 48 h after infection. Aliquots were taken at several steps of the affinity and anion exchange chromatography and analyzed by SDS-PAGE and Coomassie staining. Imidazole concentration in wash buffers was 0, 10, 20, and 0 mM in Ni-NTA wash buffers 1,2,3, and 4, respectively. Eluate fractions 1–7 were pooled and diluted ~7-fold to reduce salt and allow binding to the anion exchange resin. The solution was applied to an anion exchange column (load, L). Flow through (FT) and wash (W) were collected before fractionated elution with a linear 0–1 M NaCl gradient. Fractions were analyzed both undiluted (upper right gel) to assess purity, and diluted for initial yield estimation *via* comparison with BSA standards (0.2–1 μg).

p110γ or p87^{PIKAP} due to unmatched expression levels. Purified His-tagged p110γ was assayed as a control for the behavior of monomeric p110γ on the gel filtration column. In all fractions assayed (11–13), a single elution peak was obtained in fractions prior to those that contained the monomeric protein in the control run (data not shown). These data indicate that the prepared protein is present in a dimeric form, although in principle it cannot be ruled out that homodimers of p110γ or p87^{PIKAP} were detected.

In collaboration with the crystallography group of Prof. Heinemann at the Max Delbrück Center Berlin, the size distribution of particles present in the preparation was assessed by dynamic light scattering (DLS). In a light scattering measurement, the hydrodynamic radius of a particle can be derived from fluctuations in the intensity of the scattered light, which are caused by Brownian motion of the particles. The pooled fractions 11–13 of the preparation exhibited

a single population of particles with a mean size of ~400 kDa (data not shown). Although the preparation was monodisperse – a prerequisite for crystallization – the calculated particle size did not match the expected molecular weight. The reason for this may lie in a significant deviation from the globular shape assumed in the calculation or may reflect the formation of 'dimers of dimers'. A standard initial screen with 594 conditions was set up with this protein, but yielded no crystals so far.

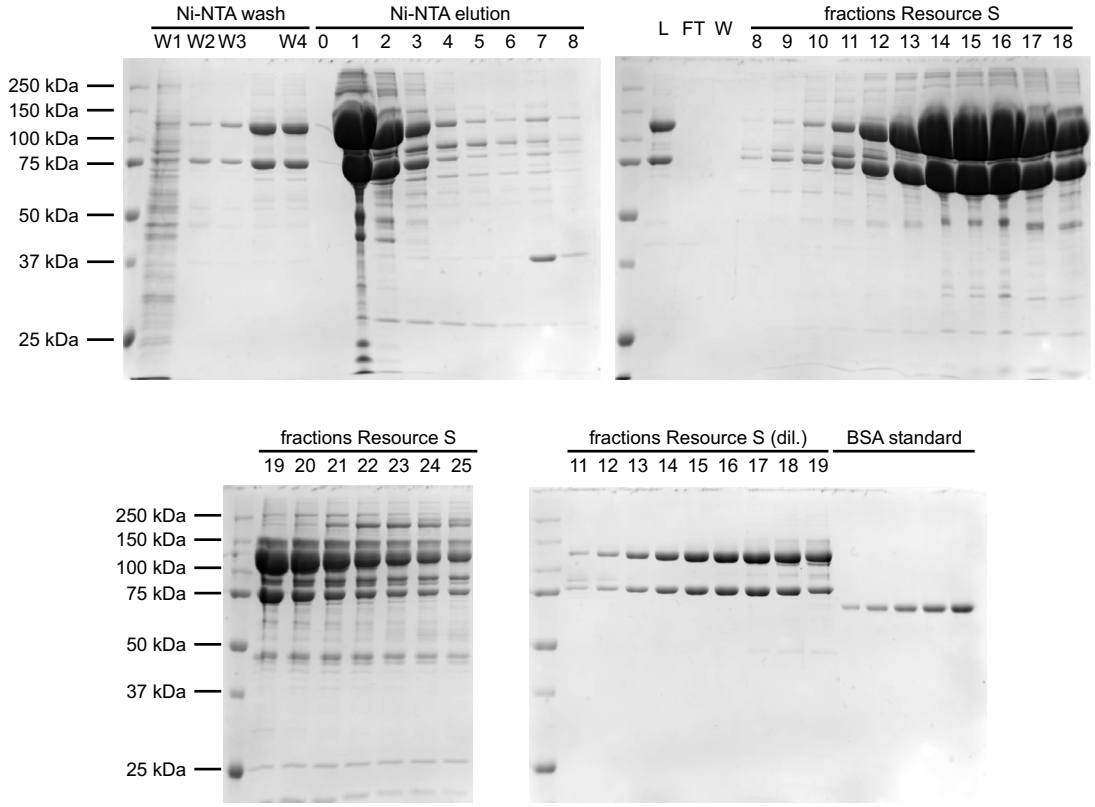

Figure 4.44: Purification of singly-His-tagged heterodimeric p110γ/p87^{PIKAP} complexes from Sf21 cells. Sf21 cells were infected with baculoviruses encoding wild-type p87^{PIKAP} and p110γ N-terminally fused to an TEV protease-cleavable His tag. Cell lysates were prepared 48 h after infection. The purification consisting of Ni-NTA affinity and cation exchange chromatography was monitored at several steps by SDS-PAGE and Coomassie staining. Imidazole concentration in wash buffers was 0, 10, 20, and 0 mM in Ni-NTA wash buffers 1,2,3, and 4, respectively. Eluate fractions 1–3 were pooled and diluted 10-fold to reduce salt concentration for the following cation exchange step (see load, L). Flow through (FT) and wash (W) were collected before fractionated elution with a linear 0.075–1 M NaCl gradient. Fractions were analyzed both undiluted (upper right gel and lower left gel) to assess purity, and diluted for initial yield estimation *via* comparison with BSA standards (0.2–1 μg, lower right gel).

Because the presumably unstructured His tags may interfere with the adoption of a higher order crystalline array, it was tried to remove the tags by proteolytic digestion with factor Xa. A corresponding recognition site had been introduced in the constructs C-terminally of the His

tag. Unfortunately, factor Xa proved to act rather promiscuous, resulting in unspecific digestion of both proteins to multiple fragments of lower molecular weight (data not shown). To reduce the need for removal of the His tag and to facilitate its removal if still required, new baculovirus constructs were prepared encoding wild-type, His tag-free p87^{PIKAP} and p110γ with an N-terminal His tag that is cleavable by TEV protease. The presence of His tags at the N-termini of both p110γ and p87^{PIKAP} may have resulted in an especially cumbersome arrangement that precludes the adoption of a stable conformation of the far N termini in both proteins. Thus, it was considered reasonable to first attempt crystallization using the heterodimer containing only a single His tag.

In contrast to the previously employed dimer, elution of singly His-tagged p110γ/p87^{PIKAP} dimer from the Ni-NTA column was characterized by a much sharper peak (Fig. 4.44). For the second round of purification, a cation exchange step was employed instead of the anion exchange chromatography in order to test whether better purity may be obtained. Moreover, it allowed to use a buffer with more physiological pH (pH 7, below the theoretical isoelectric point of 7.8) than that necessary for binding to the anion exchange resin (buffer at pH 8.4). The fractions containing the peak of eluted PI3Kγ dimer showed comparable or even slightly better purity than those previously obtained (Fig. 4.44, upper right gel). Analytic gel filtration showed that only a single species corresponding to dimeric protein was present in the peak fractions, and dynamic light scattering revealed a monodisperse solution containing particles of ~240 kDa size (data not shown). This size was in good agreement with the molecular weight of the complex. Crystallization screens have been initiated and are still under observation.